

POLITECNICO DI TORINO

Corso di Laurea Magistrale in Ingegneria Civile



Tesi di Laurea Magistrale

EVALUATION OF CRACK WIDTH DUE TO CORROSION IN RC AND PC STRUCTURES

Relatore:

Francesco Tondolo

Candidato:

Paola Costa

Correlatore:

Pierclaudio Savino

Anno Accademico: 2019/2020

INDEX

INTRODUCTION	4
1. REINFORCED CONCRETE AND PRESTRESSED CONCRETE STRUCTURES	6
2. CORROSION	10
2.1. GENERAL CONCEPT OF DURABILITY	10
2.2. CORROSION OF THE REINFORCEMENTS	11
2.3. CARBONATION	13
2.4. CORROSION FROM CHLORIDES	18
2.5. OTHER TYPES OF CORROSION	21
2.6. FROST AND THAW CYCLES	23
3. TECHNIQUES FOR THE DIAGNOSIS OF REINFORCEMENT CORROSION	25
3.1. NON-DESTRUCTIVE IN SITU DIAGNOSTIC TECHNIQUES	25
3.1.1. <i>Electrochemical tests on the reinforcements</i>	25
3.1.2. <i>Tests for the estimation of mechanical properties</i>	27
3.1.3. <i>Other non-destructive and semi-destructive tests</i>	31
3.2. DESTRUCTIVE TESTS	33
4. MODELS FOR CORROSION-INDUCED CRACKING	35
4.1. CONNECTION BETWEEN CORROSION AND PRESTRESSING	35
4.1.1. <i>The micro-crack formation stage</i>	35
4.1.2. <i>Cover cracking initiation stage</i>	38
4.1.3. <i>Crack width growth stage</i>	39
4.1.4. <i>Model verification</i>	40
4.2. THE EFFECT OF STIRRUPS ON THE FILLING OF CORROSION PRODUCTS AND CONCRETE CRACKING	42
4.2.1. <i>Specimens details and accelerated corrosion of strand</i>	42
4.2.2. <i>Prediction Model of Crack Propagation</i>	44
4.2.3. <i>Conclusions</i>	46
5. CONCRETE CRACKING PREDICTION UNDER COMBINED PRESTRESS AND STRAND CORROSION	48
5.1. EXPERIMENTAL PROGRAM	48
5.2. EXPERIMENTAL RESULTS AND DISCUSSION	51
5.3. ANALYTICAL MODEL TO PREDICT THE PC CRACKING FROM INITIATION TO PROPAGATION	

5.4.	IMPLEMENTATION OF THE ANALYTICAL MODEL AND EVALUATION OF THE RESULTS	64
5.5.	COMPARISON WITH THE EXPERIMENTAL RESULTS	66
5.5.1.	<i>Results</i>	67
5.6.	EXPERIMENTAL RESULTS PRESENT IN THE LITERATURE AND INTRODUCTION OF A NEW INTERPOLATION FUNCTION	70
5.6.1.	<i>Comparison between the analytical model and experimental data present in literature</i>	74
5.7.	APPLICATION OF THE ANALYTICAL MODEL ON CORRODED PC STRUCTURES.	76
5.7.1.	<i>Assessment of cracking time</i>	78
5.7.2.	<i>Abacus to assess the level of corrosion in PC elements</i>	81
	CONCLUSIONS	84
	APPENDIX	87
	ACKNOWLEDGMENTS	88
	INDEX OF FIGURES	89
	INDEX OF TABLES	91
	BIBLIOGRAPHY	92

INTRODUCTION

Until the late 1970s, reinforced concrete structures are believed to be intrinsically durable even if exposed to normally aggressive environments. In more recent years in the face of increasing cases of degradation the perspective has drastically changed.

Chloride-induced steel corrosion has been identified as one of the most prevalent deterioration factors in concrete structures and in recent years deterioration caused by strand corrosion has been also found in some existing prestressed concrete (PC) structures.

A considerable amount of studies have been undertaken on corrosion-induced cracking of reinforced concrete (RC) structures and these studies can be divided into three categories: empirical models, numerical models and analytical models. On the other hand, very few works examine in depth corrosion-induced cracking of PC beams. The long-term performance deterioration is another subject where developments are still ongoing; the aim of this study is to discuss and deepen the phenomenon providing additional knowledge in such field.

Concrete cracking degrades the stiffness and capacity of structures, therefore the corrosion induced cracking is a key element to ensure the serviceability and safety of PC structures.

In the present work a model based on thick-walled cylinder theory is used to represent concrete cracking induced by prestress strand corrosion. In order to take into account the concrete cohesive contribution, a reduction stiffness parameter is introduced based on fracture energy theory. The effect of both expansion ratio of strand corrosion products and crack propagation under various prestress conditions will be discussed. The analytical model is tested to predict the global process of RC and PC cracking from initiation to propagation. In this thesis work the model is implemented with a calculation code in MATLAB language and it is validated comparing with experimental results. Finally, a tool was also created that can be used for monitoring the RC and PC structures.

1. Reinforced concrete and prestressed concrete structures

Reinforced concrete is a composite material based on the bond between concrete and steel reinforcements, this bond is obtained thanks to the adherence of the cement binder and the aggregate interlock action. Concrete has a high compressive strength but a low tensile strength, so in traction the reinforcing bars are arranged on the side where there are traction tensions. Instead in the compressed structures the cement conglomerate is used to increase the compression bearing capacity.

The concrete-steel combination works well for several reasons : the two elements have an equal expansion coefficient (about $10^{-5} \text{ }^{\circ}\text{C}^{-1}$); concrete protects steel bars from corrosion as it creates a basic environment that prevents oxidation; concrete protects the reinforcement bars from the fire because it delays reaching high temperatures and the consequent loss of resistance.

Reinforced concrete is widely used, below are listed the main reason of the success of this compound material:

- resistance to high compression stress and high temperatures;
- life and low maintenance costs;
- it is the most economical solution for many types of structures such as foundations, retaining walls and dams;
- structural elements of any shape can be obtained as the concrete is initially fluid and takes the form of the formwork into which it is poured;
- it is possible to create structural elements with high rigidity without deformability problems.
- construction of monolithic structures even with castings made at different times. Thanks to particular reinforcements works undertaken at different times behave like monolithic structures, so the structure gain a higher hyperstatic degree improving the behaviour in the presence of scenarios of exceptional load.

On the other hand, there are some downsides to be considered:

- the cost of the formwork which represents about 20 % of the total cost;
- the final performance of the material is highly influenced by the mix design and the curing process;
- the incidence of dead load is very high and is generally around the 40% in civil buildings. From a design point of view, it lead to an iterative procedure where dimensions of the elements are initially hypothesised and then verified, increasing design time and uncertainties;
- due to the small tensile resistance, cracks are unavoidable and arise even in the absence of load;
- the displacements evolve over time due to viscous deformation, which is the material's characteristic to deform in the presence of constant load;
- high dismantling costs and low eco-sustainability.

In order to improve the behaviour of reinforced concrete structures and minimise the downsides listed above, precompression can be used. This method consists of introducing a tensional state opposite to the tensile force which will exist when the element will be in service. Introducing a state of compression into the element, the resulting traction tensions, is drastically reduced or can even turned into a global state of compression.

Figure 1.1 shows the effect of the precompression on a supported beam.

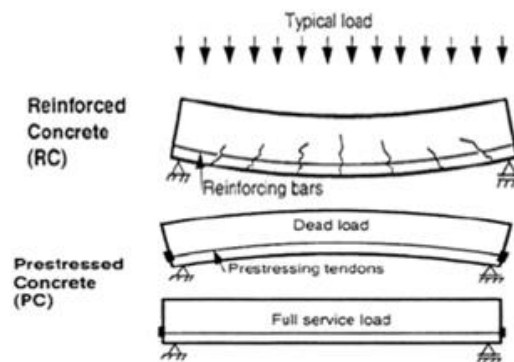


Figure 1.1 Prestress effect on a supported beam [9]

In prestressed elements the crack width should be drastically reduced, and if correctly calculated, the tensile stress cancelled.

In the section analysis of ordinary reinforced concrete, at the second and third stages, the contribution of the stretched part is neglected, leaving the task of resisting traction exclusively to the reinforcement. The prestress process is then used to optimise sections in order to be completely reactive.

Steel is then arranged in different configuration to absorb different degree of stress. The most common arrangement is : wire (full section material), braid (set of two or three wires wound around the axis), strand (set of wires wound around a central rectilinear wire, in one or more crowns) and bar (element with full section greater than the wire).

The prestressed reinforced concrete has considerable applications in the building sector, both in civil and hydraulic constructions. While the reinforced concrete allows to reach a maximum span of 6 m (about 7 m if using prefabricated elements), the prestressed reinforced concrete allows to produce beams over 12 m long.

Prestressed element cannot only be produced in factories but also directly on site. Both for hydraulic and building use, the elements in P.R.C. can be realised

following two main production methods, respectively with pre-tensioned or post-tensioned reinforcement.

While during the pre-tensioning process, steel is stretched before the concrete casting, in the post-tensioning the stretching occurs after the concrete casting, therefore in the initial phase it is necessary to insert some ducts in order to make the steel independent from the concrete.

The post-tensioning system is more expensive than the pre-tension but has two important advantages:

- the elements can be entirely realised on site, solving the problem to transport large elements;
- the possibility to choose the path unlike the pre-tensioning where the path is necessarily straight.

2. Corrosion

2.1. General concept of durability

In civil engineering, durability is a key aspect that has been introduced in the last twenty years. Over the years it became also clear that the fundamental problem of the durability of reinforced concrete, refers to the corrosion of the reinforcements inside it.

Durability indicates the conservation over time of the physical and mechanical characteristics of material and structure. Durability of the material is the ability to last over time and resist the aggressive actions of the surrounding environment. The durability of the structure is more relevant and is the ability to guarantee the service for which the structure is designed and the relative safety for the expected life period.

Structures must reach certain characteristics of deformability, cracking, probability of failure etc. and must maintain them over time to be durable.

Time is not unlimited, but any structure is designed for a certain expected life span in relation to which actions and resistances are defined. Table 1 shows the key values:

Description	Time (years)
Ordinary structures	50
Important structures	100
Fundamental structures (e.g. nuclear power plants)	200

Table 1 Expected life period [9]

The durability of the material is necessary but not sufficient condition to guarantee the durability of the structure, this is due to the presence of causes of structural degradation not attributable to the low durability of the material.

It is clear that to reduce the number, extension and severity of the maintenance interventions it is necessary to limit the effect of the penetration of potentially aggressive substances. In reinforced concrete structures exposed in natural environments there are situations that accelerate the degradation process of the concrete, the most important are:

- contact with aggressive chemical substances;
- corrosion of reinforcements;
- frost and thaw cycles.

2.2. Corrosion of the reinforcements

A reason for the success of reinforced concrete structures is the protection that the concrete makes towards the reinforcement. In fact, the concrete creates a basic environment in which a thin film of ferric oxide forms on the steel that protects from galvanic corrosion: this phenomenon is called passivation.

When the pH drops to 12 the passivating layer that forms on the bar may be altered and may cause the breakage of the protective film, hence corrosion can occur under certain environmental conditions. The corrosion process of steel, how is shown in the figure 2.1, is an electrochemical phenomenon in which two areas with different electrochemical potential are formed on the metal surface, these are anode and cathode.

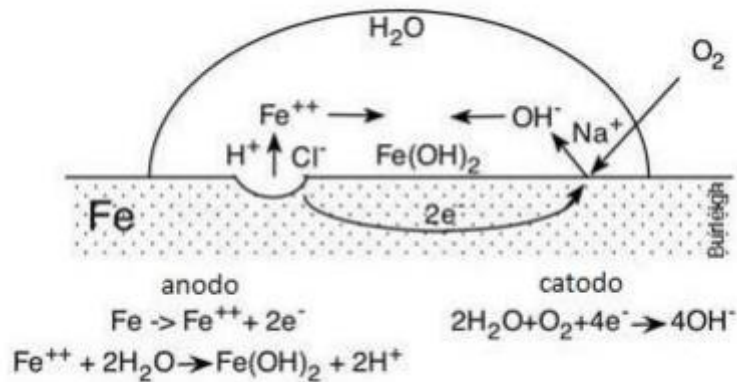


Figure 2.1 Simplified mechanism of steel corrosion in aqueous medium: anodic e cathodic zone

There are three processes that occur during corrosion:

- the anodic metal oxidation reaction, which forms the products of corrosion and produces electrons in the crystal lattice;
- the cathodic semi-reaction that reduces the oxygen present in the aggressive environment and consumes the electrons produced in the anodic process;
- the circulation of current in the metal with a flow of electrons in the crystal lattice;

In degraded structures it is possible to directly notice the reinforcing bars, in fact the corrosion has reduced the resistant section causing a reduction of the bearing capacity of the element. Corrosion consists in the oxidation of the reinforcing bar and the oxide occupies a greater volume than the original steel. As the oxidation progresses, pressures arise towards the outside due to the increase in volume of the oxidized bars. These pressures locally send the concrete in compression and longitudinal cracks arise parallel to the bars. In the long time there are swellings and detachments of the cover that more expose the reinforcement and worsen the situation. In figure 2.2 it is possible to see an example of degraded elements due to corrosion.



Figure 2.2 Example of degradation due to corrosion [16]

There are two important environmental factors that promote the corrosion process: carbonation and the presence of chlorides. Depending on the extent of the attacked area, corrosion is mainly divided into two categories:

- diffuse corrosion, if the phenomenon is widespread and uniform, or when the penetration is the same throughout the development of the element. An example is carbonation corrosion;
- pitting corrosion, when it appears as mainly localized attacks that from the surface penetrate into the thickness of the metal, often at high speeds. With chlorides the damage is localized, insidious and difficult to find and therefore the danger is greater.

2.3. Carbonation

It is a chemical phenomenon that varies the chemical composition of concrete in direct contact with carbon dioxide.

As there is a reduction in the pH, the passivating film can break and in the presence of other environmental conditions it can cause corrosion.

It is shown that carbon dioxide penetrates inside the concrete according to a root law:

$$s = k\sqrt{t} \quad (2.1)$$

Where s is the thickness of the carbonated layer in mm, k is the carbonation coefficient [mm / year^{1/2}], n is a coefficient generally set equal to 2 (average porous concretes) and t is the time in years. By appropriately estimating the k coefficient it is possible to evaluate the progression of the carbonated front as shown in the figure 2.3.

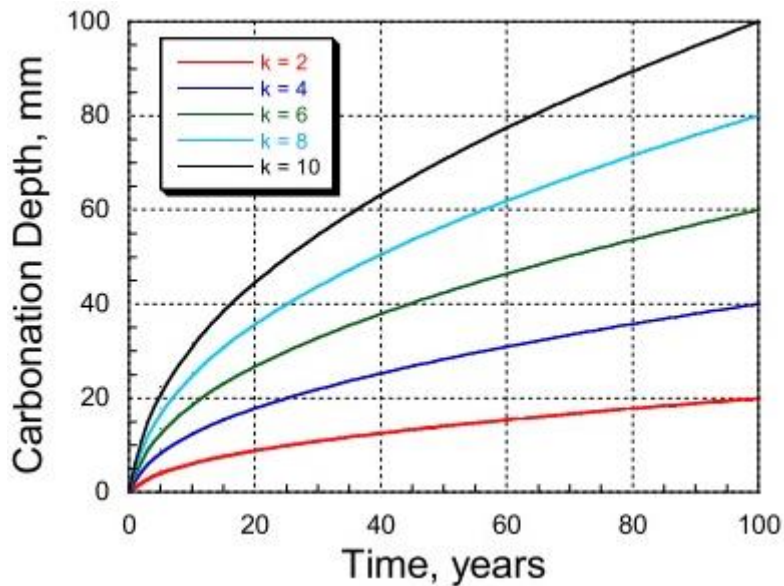


Figure 2.3 Evolution of the carbonated front as a function of k and t

By the phenolphthalein tests it is possible to estimate the coefficient k and then calculate the time remaining for the activation of the corrosion phenomenon. The procedure uses the properties of the reagent that changes colour on contact with the concrete having $\text{pH} > 8.0 \div 9.8$ and remaining colourless for lower pH values. The determination of the carbonation depth, which must be carried out immediately after taking the sample, it is done by spraying the phenolphthalein solution on the

test piece. The carbonated concrete does not change its colour, while the one not yet reached by carbonation takes on the typical magenta red colour of the reagent in an alkaline environment. Phenolphthalein tests is shown in the figure 2.4.



Figure 2.4 Determination of the carbonated front using the phenolphthalein test

During the carbonation process, water and carbon dioxide present in the atmosphere gradually penetrate inside the structure and the carbonated part increases. When it arrives at the armature, the passivating film can break and in the presence of other causes corrosion can start. As the corrosion continues, a longitudinal slit arises from the armature towards the outside that follows parallel to the bar. Looking at the evolution of the penetration depth as a function of time, as shown in figure 2.5, with the same conditions and with the variation of the water/cement ratio, the trend changes and, increasing water/cement ratio the penetration depth increases.

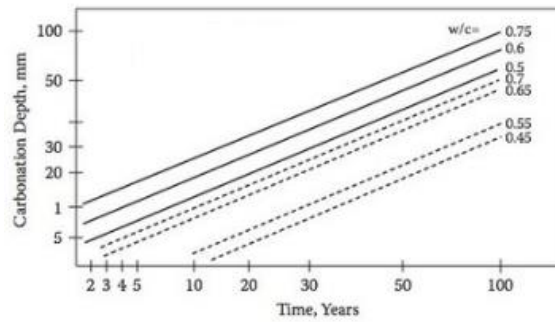


Figure 2.5 Depth of corrosion penetration

From the results shown in figure 2.5, it can be deduced that an obvious solution is to reduce the water/concrete ratio, in this way the concrete is more resistant, less porous and less carbon dioxide can go through delaying the carbonation process. On the other hand, if the pores are completely saturated, carbon dioxide has difficulty moving, so with structures immersed in water there is no carbonation. As the relative humidity changes, the carbonation rate increases until it reaches a peak in correspondence with the ambient humidity, after which it drops rapidly until it is zero, therefore there is a danger interval between 50 and 80%. Figure 2.6 shows the behaviour mentioned above.

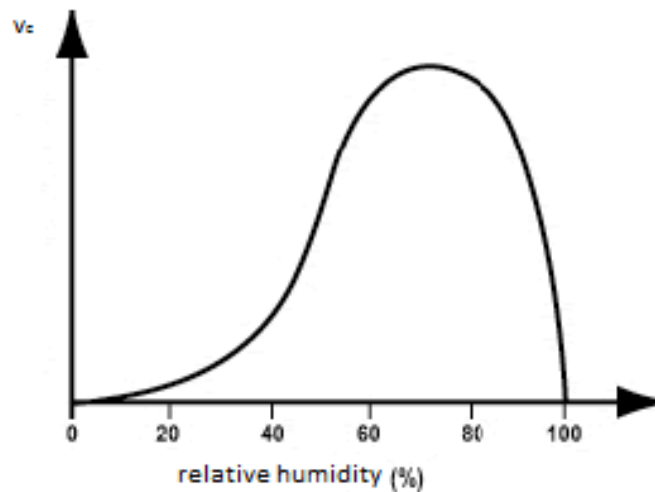


Figure 2.6 Carbonation speed according to relative humidity

The UNI EN 206 standard defines different exposure classes:

CORROSION INDUCED BY CARBONATION		
XC1	Dry or permanently wet	-Concrete inside buildings with low air humidity -Concrete permanently submerged in water
XC2	Wet, rarely dry	-Concrete surfaces in contact with water for long periods -Foundations
XC3	Moderate humidity	-Concrete inside buildings with a high / moderate low air humidity -Concrete located outside not subject to rain
XC4	Subject to dry and wet cycles	-Concrete surfaces in contact with water

Table 2 Classification of corrosion levels proposed by the UNI EN 206 standard

In general terms, the carbonation evolution depends on the following parameters:

- relative humidity: it is the most important parameter that affects the carbonation. Carbon dioxide is a gas and because it is soluble in water its access is promoted in presence of high levels of relative humidity. On the other hand, carbon dioxide, being a gas, diffuses easily in the empty pores. In presence of saturated concrete the diffusion speed is slowed down. In light of these reasons carbonation speed is considerably high for 50-80% of relative humidity.
- carbon dioxide concentration: more the CO₂ concentration increases, faster is the diffusion of carbonation.

- temperature: temperature increase causes the speed-up of carbonation penetration.
- w/c ratio: the penetration speed depends on concrete permeability and porosity.
- concrete alkalinity: the higher the alkalinity of concrete, the higher carbonation process should be carried out. Concrete alkalinity depends basically on the mixture and on the cement type.

Finally, in order to occur corrosion, three factors must be concomitantly:

- carbonation that surpasses steel;
- presence of oxygen;
- intermittent presence of water that allows corrosion and when there is no water it allows carbonation to progress;

The solutions are mainly the waterproofing of the surfaces to limit the entry of water and carbon dioxide or increase the cover to extend the corrosion process.

2.4. Corrosion from chlorides

The corrosion from chlorides, is another phenomenon that breaks the protective film and causes the corrosion of the reinforcement. Traces of chlorides can be found within the concrete mix, or in any external environment since the structure can be in direct contact with sea, brackish water, marine aerosol or de-icing salts.

The evolution of the phenomenon, as shown in figure 2.7, is similar to carbonation and a critical chloride content is defined: if the chloride ions are below this level there is no corrosion because the film is not affected, when they penetrate, the area where the content is exceeded increases more and more until it reaches the reinforcement and begin corrosion.

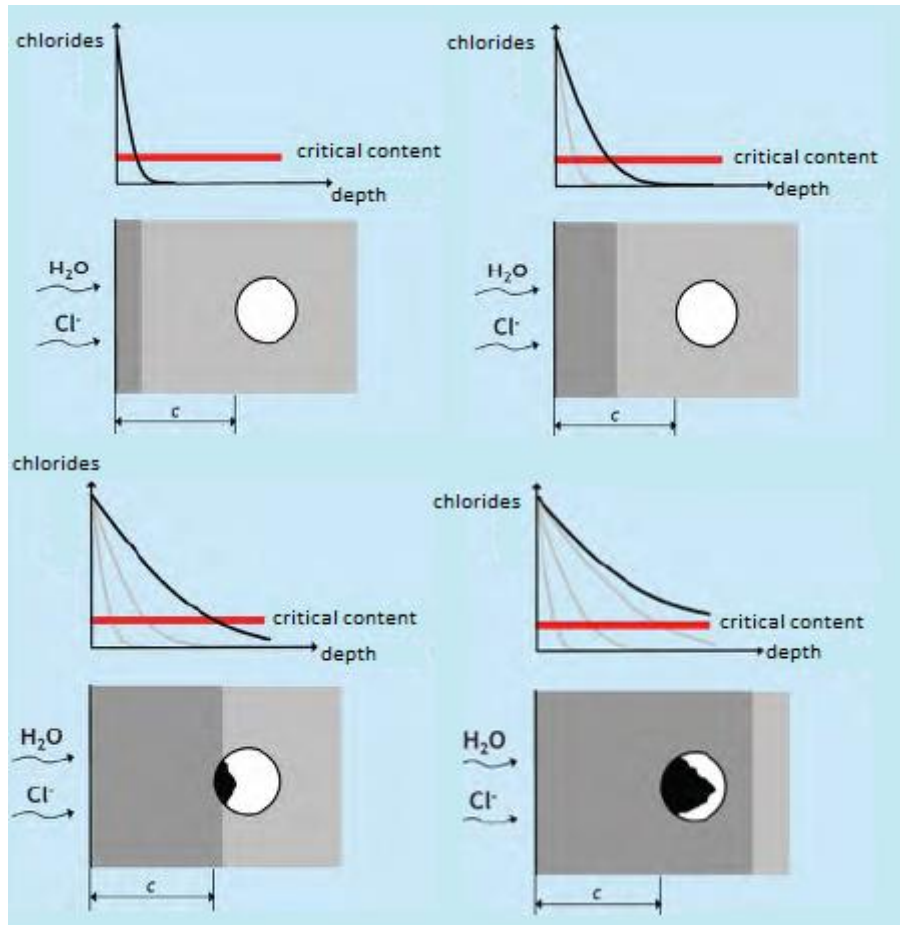


Figure 2.7 Corrosion initiation process [8]

The aforementioned ions punctually destroy the passivating film and craters are created at the anode of the electrochemical cell, this leads to corrosion called pitting as shown in figure 2.8.



Figure 2.8 pitting corrosion [8]

Chloride ions can already be present in the mixture or come from the outside or penetrate inside through the network of pores and reach the reinforcement. While the first are not very common, as long as the recommendations on the use of pure, non-marine waters, etc. are respected, the presence of the second is much more frequent especially in marine environments or in winter due to the use of anti-freeze salts on the roads. The amount of chlorides needed to trigger corrosion depends on various factors:

- water / cement ratio;
- type of cement;
- hardening and compacting of the concrete;
- availability of oxygen.
- moisture content;
- type and surface of reinforcing steel;

The number of such factors makes it difficult to define a limit for the chloride content, below which it is certain that depassivation of the protective film will not occur. A generally accepted value for the maximum chloride content of concrete is 0.4% in relation to the weight of the cement, or 0.05 to 0.1% in relation to the weight of the concrete. In recent decades, numerous models have been proposed to describe the process related to the penetration of chlorides into the concrete. Many of them include a large number of parameters dependent on numerous factors, which can only be deduced experimentally and with a large degree of uncertainty. For this reason, semiempirical models, which take the entry of chlorides as a pure diffusion process, are the most used ones. This hypothesis can be described by Fick's second diffusion law:

$$\frac{\partial C}{\partial t} = D \frac{\partial^2 C}{\partial x^2} \quad (2.2)$$

where C is the total concentration of chloride ions at the distance x from the surface after a time t of exposure to chlorides and D the diffusion coefficient of chloride.

Assuming that the chloride concentration on the surface remains constant over time, the solution of equation (1) is provided by (2):

$$C(x, t) = C_0 + (C_{s, \Delta x} - C_0) \left[1 - \operatorname{erf} \left(\frac{x - \Delta_x}{2\sqrt{D_{app,c} * t}} \right) \right] \quad (2.3)$$

with:

$C(x, t)$ concentration of chloride at depth x from the external surface at a given instant of time t , in% of the cement mass;

- $D_{app,c}$ is the apparent diffusion coefficient of chloride in concrete, in m^2 / s ;

- $C_{s, \Delta x}$ chloride concentration at the depth of Δ_x , in% of the cement mass;

- C_0 initial chloride concentration of the concrete, in% of the cement mass; x depth, in m; Δ_x depth of the convection zone, in m;

- t concrete age, in s;

- $\operatorname{erf}()$ is the function of Gauss errors. The probability of ignition chloride-induced corrosion, P_{corr} , is time-dependent and can be expressed as:

$$P_{corr}(t) = \Pr[C_{crit} - C(x = c, t) < 0] \quad (2.4)$$

where C_{crit} is the chloride concentration limit and C the cover thickness. The value of C_{crit} is defined as the total content of chloride which leads to the depassivation of the surface of the reinforcement and therefore to the triggering of the corrosion of the metal.

2.5. Other types of corrosion

Other types of corrosion exist although they are not so common in RC structures.

- fatigue corrosion, in general, occurs in high-strength reinforcement, therefore in prestressed concrete structures; it is closely related to the phenomenon known as hydrogen embrittlement which, under particular conditions (metallurgical, environmental and loading), is responsible for a brittle fracture of the material.

Hydrogen embrittlement is the process by which hydrogen diffuses into the metal matrix and alter the metal characteristic into a brittle material.

- corrosion due to induced currents could arise in railway structures, bridges, tunnels, or structures adjacent to them; in these cases we could detect the presence of electric currents that do not follow their own paths, disperse in the reinforced concrete and go to affect areas of the bars in more or less distant areas; the effects, which are negligible in the presence of alternating currents, can be significant in the presence of continuous currents, with great intensity and prolonged over time, destroying the passivating state of the reinforcement in the areas where the transition to concrete takes place.
- galvanic corrosion: it occurs when two or more metals of different nature, or even of the same nature, are mated but with a different internal structure, in the presence of a humid environment.

Each metal or alloy has its own electric potential based on its chemical composition and therefore in relation to the environment in which it is located has the ability to receive or transfer electrons. If the difference between the different electric potentials, in the presence of an acid solution, exceeds a certain threshold, a passage of electrons is created between a donor (anode) and a receptor (cathode) and the intensity of this movement of electrons will be greater the greater the difference in electrical potential. This movement of electrons represents a real electric current called galvanic current which triggers the corrosion process and the anode, which releases electrons, oxidizes at an ever increasing speed as the ratio between the useful area of the anode and that of the cathodic zone is always smaller.

- cavitation corrosion is caused by the formation and consequent collapse of air bubbles or cavities filled with steam, inside a liquid in contact with metal surfaces. It occurs in particular on metal surfaces when the flow rate of the liquid is high or in the presence of pressure variations. For example, centrifugal pumps and ship propellers are most affected.

- crack corrosion (also known as crevice corrosion) is a type of localized corrosion that can occur in cracks or below screened surfaces in which there may be stagnant solutions.

It occurs mainly on "objects" such as gaskets, nails, bolts or under porous deposits. There are many alloys most affected by crack corrosion: among these are stainless steels, titanium, aluminum and copper alloys. This is a localized form of corrosion that occurs in limited areas to which the access of the gas or fluid is limited. In this context very aggressive micro environments can develop and localized oxidation could be further accelerated.

- intergranular corrosion is a localized corrosion in the grain boundaries of the crystal lattice that for thermal reasons, such as welding and heat treatment, is sensitized and therefore sensitive to aggressive attacks of particular corrosive agents as the percentage of chromium is insufficient for the creation of the film protective oxide.

The intergranular corrosion creates micro cracks nearby the grain which could be emphasized in presence of stresses.

- fretting corrosion occurs at the interface of materials that are subject to vibrations and small sliding under load, causing the formation of furrows or pitting surrounded by corrosion products or sometimes (in the case of metals) even just loss of gloss. In the case of metals, precisely, it happens that the fragments between the surfaces in contact are oxidized and parts of the oxide film (film) are removed.

2.6. Frost and thaw cycles

In the liquid-solid transition, water increases its volume by approximately 9%. The cycles of volume change can damage the concrete, but the problem is difficult to solve, and the interventions can be:

- to prevent the entry of water and to avoid water surpluses during construction;
- an adequate system of micro bubbles of air is inserted that leaves a space that will be occupied by the water when it will increase in volume.

3. Techniques for the diagnosis of reinforcement corrosion

3.1. Non-destructive in situ diagnostic techniques

Non-destructive techniques are a set of diagnostic practices designed to detect the characteristics of the materials in use and to assess anomalies, defects and state of degradation without altering their physical state or geometry. In this regard, non-destructive investigations, and more generally all the methods used in the diagnostics and monitoring sector, play a fundamental role both for the control of the degradation of materials and for the evaluation of the quality and reliability of the products. Several variables affect the inspection results:

- the identification of the most suitable analysis methodologies for the specificity of the case;
- the qualification of the control procedures;
- the instrumental and functional characteristics of the equipment used and the products used;
- the execution of the tests in a targeted manner or executed only in areas where the most disadvantageous exposure conditions are detected.

3.1.1. Electrochemical tests on the reinforcements

The electrochemical tests are essentially: measurement of the corrosion potential, mapping of the potential in the direction of the bars, resistivity measurements and measurement of the corrosion rate of the reinforcements.

The first method makes it possible to identify the areas in which the reinforcements are close to the phenomenon of corrosion or have already started the degradation process and those where the attack is excluded. The in situ carried out by detecting the potential of the reinforcement with respect to a reference electrode placed in

contact with the surface of the concrete by means of a sponge soaked in water and with copper sulphate copper electrode.

The potential mapping, shown in the figure 3.1, allows:

- to identify corrosion before its effects are visible;
- to classify homogeneous reinforced concrete structures according to the state of corrosion of the reinforcements and to the extension of the attacks, also for the purpose of establishing intervention priorities;
- integrated with other techniques, in particular chemical analyses on concrete cores, to identify the causes of corrosion in order to design the most suitable restoration interventions;
- repeated at fixed intervals (2-3 years), it allows to monitor the onset and progress of corrosion over time.

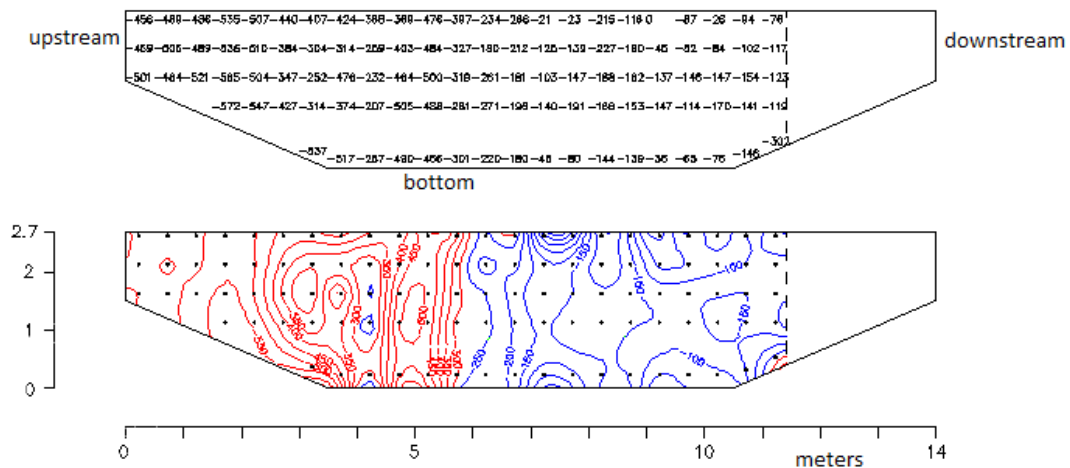


Figure 3.1 Example of potential mapping

The resistivity measurements of concrete, with the exception of passive reinforcement, can be directly linked to the corrosion rate of the reinforcements.

It can be assumed that in the propagation period the corrosion rate is negligible for resistivity greater than 1000 Ωm , low for 1000-500 Ωm , moderate for 500-100 Ωm and high for resistivity less than 100 Ωm .

The resistivity measurement is obtained using the "four electrode" method, or Wenner's method. The difference in potential, E , is present between two electrodes positioned between the reinforcements. The ratio, E / I , where I is the supply current, allows to obtain the value of the resistivity, unless a geometric factor depends on the distance between the electrodes. The resistivity measurement is especially useful to identify, within a structure, the areas of greatest corrosion or to evaluate the variations suffered by the concrete over time, i.e. the penetration of chlorides or carbonation.

Finally, the measurement of linear polarization is another way to evaluate the corrosion rate of the reinforcements.

This method involves the use of three electrodes: working electrode, W , or the metal to be evaluated, the reference electrode, RE , and a counter-electrode, CE , which has the function of delivering current during the test (Figure 3.2).

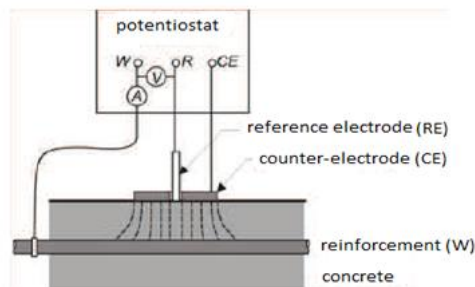


Figure 3.2 Schematic illustration of linear polarization measurements

3.1.2. Tests for the estimation of mechanical properties

Non-destructive techniques can be used to determine the properties of hardened concrete, to identify defects or discontinuities, to assess the condition of concrete structures, and therefore to check the level of concrete degradation in general. These techniques do not provide a direct measure of a mechanical property of concrete, but it is necessary to know the correlation between the result provided by the test and the property to be estimated.

The most significant tests for the estimation of mechanical properties are: the sclerometric tests and the ultrasonic velocity measurement tests

The sclerometric survey, or sclerometric test, is a non-destructive test for the determination of the rebound index of an area of hardened concrete using a steel hammer driven by a spring, known as a Schmidt hammer or sclerometer.

The test is based on the correspondence existing between the unitary load of compression breaking and the surface hardness of the concrete, the latter measured in terms of residual elastic energy following the impact of a mobile mass with the surface of the element to be investigated. The extent of the rebound is measured by an index that runs along a graduated scale on the instrument. This test is regulated by UNI EN 12504-2: 2012 (September 2012 edition) "Test on the hardened concrete in the structures - Non-destructive tests - Determination of the sclerometric index". According to the legislation, the test must be carried out on a surface of approximately 30 x 30 cm², on which at least 9 - 10 strokes must be performed, at a distance of at least 25 mm from each other and from the outer edge, as shown in figure 3.3. The test surface must be smooth and, therefore, it must be previously sanded using an abrasive stone. The measurement can be carried out on a horizontal and vertical surface, taking care, however, to take into account the different effect of gravity acceleration on the rebound. The sclerometric measurement has little validity in the case of predicting the strength of concrete, as there is no univocal relationship between surface hardness and compressive strength.



Figure 3.3 Sclerometric tests [15]

The result of the measurement can be influenced by various factors such as:

- the type of cement;
- the type of aggregate;
- the weight content of cement;
- the surface roughness;
- the humidity conditions;
- the penetration value of the carbonation in the concrete (for example, in the presence of a significant penetration of carbonation, the sclerometric test tends to overestimate the strength of the concrete).

The ultrasonic investigation, shown in the figure 3.4, is a non-destructive investigation applied to concrete structures, by which the speed of propagation of the pulses of ultrasonic longitudinal waves in the hardened concrete is determined. The measurement of the ultrasonic pulse propagation speed can be used for the following determinations:

- uniformity of the concrete;
- presence of cracks or voids;

- casting defects;
- changes in properties over time;
- dynamic modulus of elasticity
- estimate of the strength of the concrete on site (through appropriate correlation and in combination with other non-destructive, semi-destructive or destructive tests). This test method is regulated by UNI EN 12504-4: 2005 "Tests on concrete in structures - Part 4: Determination of the propagation speed of ultrasonic pulses". Several devices constitute the equipment with which the test is conducted:

- A probe that emits pulses;
- A receiving probe that receives the impulses and transforms them into electrical signals;
- An adjustable amplification and signal processing device emitted by the receiving probe;
- A device for measuring the time interval between the moment of emission and the moment the impulse is received.

There are two methods of measuring ultrasound propagation times: Direct transmission method: consists of positioning the two probes aligned on two faces opposite to the element to be examined; Indirect transmission method: it consists in positioning the probes in different points of the same face of the element to be examined.

The surface on which the test is carried out must be clean, smooth and sufficiently flat, to allow uniform contact with the probes. On this must be applied a material, usually a gel, which avoids the presence of air between the probe and the surface of the concrete. The probes must be pressed against the concrete surface. When the emitter generates the pulses, with a frequency between 20 and 200 kHz, the value of the propagation time t must be recorded. Note the length, L , of the pulse path, in direct measurement, the speed of the pulses, v , can be calculated using appropriate formulas.



Figure 3.4 Ultrasonic tests performed on the specimens [15]

3.1.3. Other non-destructive and semi-destructive tests

The pacometric survey, shown in the figure 3.5, is a non-destructive test for the identification of the reinforcements inside the concrete castings. By means of this magnetic survey it is possible to detect with good precision the position of reinforcing bars present in the reinforced concrete members, their depth, i.e. the cover and their diameter.

This survey methodology uses the principle of measuring the absorption of the magnetic field, produced by the same pacometric device, which is highlighted by an analog or digital system coupled to an acoustic system for a more convenient search of the metal elements.



Figure 3.5 Pacometric test [15]

A method recently used, shown in the figure 3.6, is called SonReb and is the combination of two non-destructive tests carried out on the same concrete element: ultrasonic investigation and sclerometric investigation.

The strength of the concrete is estimated on the basis of the pair of values of the speed of propagation of ultrasounds and rebound index of sclerometer through the use of formulas deduced from correlations of experimental type, among which we recall: formula of Giacchetti and Lacquaniti (1980), formula by Di Leo and Pascale (1994), formula by Gasparik (1992).

The validity of the SonReb method derives from the compensation of the inaccuracies of the two non-destructive methods used. In fact, it has been noticed that the moisture content makes the sclerometric index underestimate and overestimate the speed, and that, as the age of the concrete increases, the sclerometric index increases while the ultrasonic speed decreases.



Figure 3.6 SonReb method [15]

The pull-out survey, shown in the figure 3.7, is a semi-destructive test that causes limited damage to the concrete element and is useful for determining the extraction force of a pre-embedded or post metal insert inserted in the concrete element to be tested. This test is regulated by UNI EN 12504-3: 2005 "Tests on concrete in structures - Part 3: Determination of extraction force". The test is based on the

correspondence existing between the unitary load of compression breaking of the concrete and the force necessary to extract the standardized metal insert.



Figure 3.7 Pull-out test [15]

3.2. Destructive tests

Destructive tests (or direct methods) involve the destruction of the concrete or steel sample and consist of analytical tests (chemical, physical, petrographic) or mechanical tests on samples of concrete or reinforcement taken, respectively by coring and cutting, from the existing structure.

The technique of taking cylindrical samples of hardened concrete by coring, regulated by UNI EN 12504-1: 2002 and shown in the figure 3.8, allows to obtain cores of structural material that are carefully examined, and subsequently subjected to compression test, according to normalized procedures, in order to assess the mechanical strength of concrete in situ.



Figure 3.8 Concrete samples taken by coring

The test is performed through a core drilling machine, which is a motor that rotates a core drill equipped with a water-cooled diamond crown, whose diameter used is chosen in relation to the maximum size of the aggregate present in the concrete matrix.

The extracted carrots are carefully examined and, if requested, subjected to the test of the determination of the carbonation depth: they are then marked clearly and indelibly, photographed, and finally appropriately protected and taken to the laboratory for the crushing test according to the UNI EN standard 12390-3 "Test on hardened concrete - Resistance to compression of the specimens".

Preliminary to the operation of the coring is a pacometric survey by which the reinforcing bars next to the area where the sampling is to be performed are detected, in order to exclude them from the coring path itself.

4. Models for corrosion-induced cracking

4.1. Connection between corrosion and prestressing

The phenomenon of corrosion is strongly influenced by the conditions of the structure in which it is activated.

Numerous models have been proposed to study the phenomenon of corrosion especially for reinforced concrete structures, unfortunately only in recent years the studies on prestressed structures have increased.

The first study on strand corrosion was performed by Dai et al. (2016) which proposed a global model to predict prestressed concrete cracking. The model considers three stages: micro-crack formations, cover cracking initiation and crack width growth. Using accelerated corrosion, six prestressed concrete beams were designed with different strand corrosion degree in order to obtain an experimental evidence.

In the present work, the sensitivity related to parameters such as prestress, cover, concrete tensile strength, rust expansion and strand diameter is verified.

4.1.1. The micro-crack formation stage

When the tangential stress, caused by corrosion products, is equal to the concrete tensile strength micro cracks appear. Around the strand-concrete interface, like the Figure 4.1 shows, there is a porous zone because concrete is a heterogeneous material.

Firstly, corrosion products diffused into this spongy zone, when corrosion products fill the area these products generate expansive pressure.

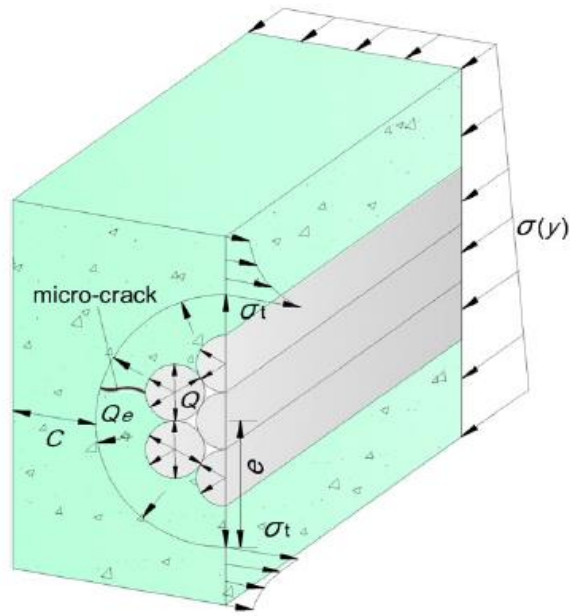


Figure 4.1 Stress distribution around the strand-concrete interface [4]

During the corrosion process concrete is under the biaxial stress state: compressive stress σ_p and tensile stress σ_t , created respectively by prestress and expansive pressure. Therefore, compressive stress is equal to:

$$\sigma_p = \frac{N_p}{A} + \frac{N_p e_p^2}{I} \quad (4.1)$$

Where A is the cross-sectional area of the concrete, I is the inertia moment of the cross section, N_p is the prestressing force of the strand and e_p is the eccentricity of the strand.

The tangential stress σ_t can be determined from:

$$\sigma_t = \frac{[(C + 3R_0)^2 + e^2]}{[(C + 3R_0)^2 - e^2]} Q_e \quad (4.2)$$

Where C is the cover, R_0 is the radius of the wire before corrosion, e is the length from the end of the micro-crack to the center of the strand and Q_e is the expansive

pressure at the end of the micro-crack. Finally, the maximum expansive pressure is calculated from the following relation:

$$Q = \left(0,225 + 0,075 \frac{C}{R_0}\right) \frac{(f_{ck} - \sigma_p) f_{tk}}{f_{ck}} \quad (4.3)$$

Where f_{ck} and f_{tk} are respectively the concrete compressive strength and the concrete tensile strength.

In this study was used seven-wire steel strand with six outer wires in contact with the surrounding concrete, as shown in the figure 4.2. Thanks to geometric considerations we can see that the contact area of the outer wire is equal to two-thirds of the surface area.

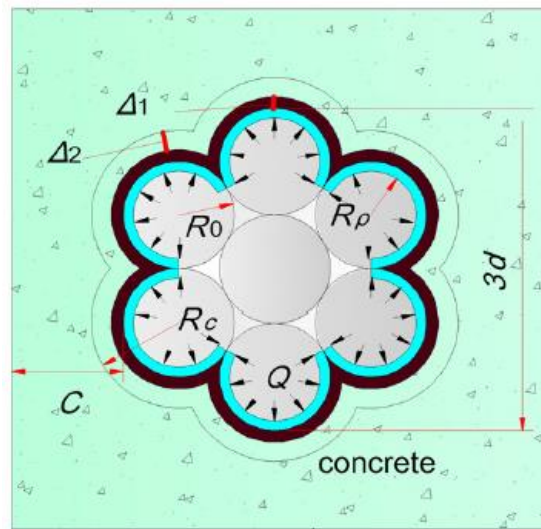


Figure 4.2 Radial deformation at the strand-concrete interface [4]

As Figure 4.2 shows, R_c is the radius of the wire with the free-expansion corrosion products, R_ρ is the residual radius of the wire after corrosion, Δ_1 is the radial deformation of the concrete and Δ_2 is the radial deformation of corrosion products.

The critical corrosion loss at the micro-crack formation ρ_m can be determined with R_c in fact:

$$R_c = \sqrt{R_0^2 + \frac{(n-1)A_p}{4\pi} \rho_m} \quad (4.4)$$

Where n is the volume ratio between corrosion products and the strand, which is referred to as the rust expansion ratio and A_p is the cross-sectional area of the strand.

4.1.2. Cover cracking initiation stage

In this stage the total volume of internal cracks V_c is calculated considering the shape of internal cracks form a triangle and the length of each crack reach the concrete surface. Figure 4.3 is a scheme of cover cracking.

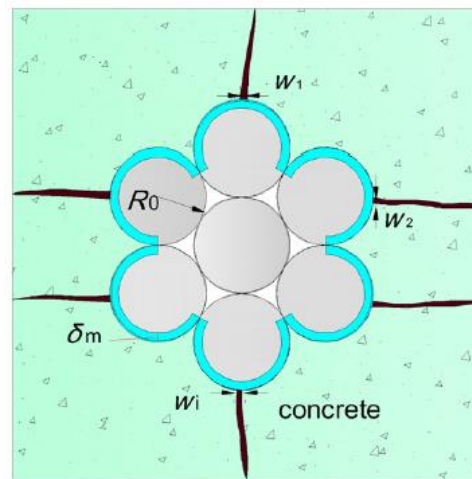


Figure 4.3 Scheme of cover cracking [4]

$$V_c = \frac{1}{2} \sum w_i C \quad (4.5)$$

Where the sum of the crack widths can be calculated as:

$$\sum w_i = 8\pi(n-1)\delta_m \quad (4.6)$$

Where δ_m is the radial loss and the radial increment of corrosion products at the strand-concrete interface is $(n - 1)\delta_m$. Therefore, the critical corrosion loss at this second stage ρ_p depends on the critical radial loss δ_p and is equal to:

$$\rho_p = \frac{4[\pi R_0^2 - \pi(R_0 - \delta_p)^2]}{A_p} \quad (4.7)$$

4.1.3. Crack width growth stage

When corrosion degree increases the crack's shape from triangular becomes rectangular in fact the visible crack propagates to the concrete surface, as shown in the figure 4.4.

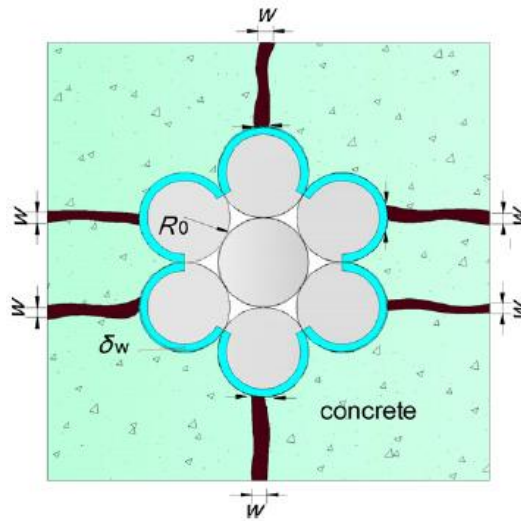


Figure 4.4 Schematic of crack width growth [4]

The relationship between radial loss at the crack width growth stage and the critical corrosion loss is equal to:

$$\rho_w = \frac{4[\pi R_0^2 - \pi(R_0 - \delta_w)^2]}{A_p} \quad (4.8)$$

4.1.4. Model verification

Six post-tensioned concrete beams were designed with accelerated corrosion-induced cracking to verify the proposed model. The artificial accelerated corrosion test, shown in Figure 4.5, was used to obtain various corrosion degrees of the strand, in fact after test a large number of longitudinal cracks were observed on the concrete surface.



Figure 4.5 Accelerated corrosion test of beams [4]

Furthermore, in this analysis, in order to study the failure load induced by the crack, a comparison was made between the failure load ratio both in reinforced and prestressed concrete structures.

Figure 4.6 shows that the flexural strength degradation caused by corrosion-induced crack is more significant in prestressed concrete structures than that in reinforced ones. It shows that corrosion-induced cracking degrades less strength of RC structures than that of PC structure.

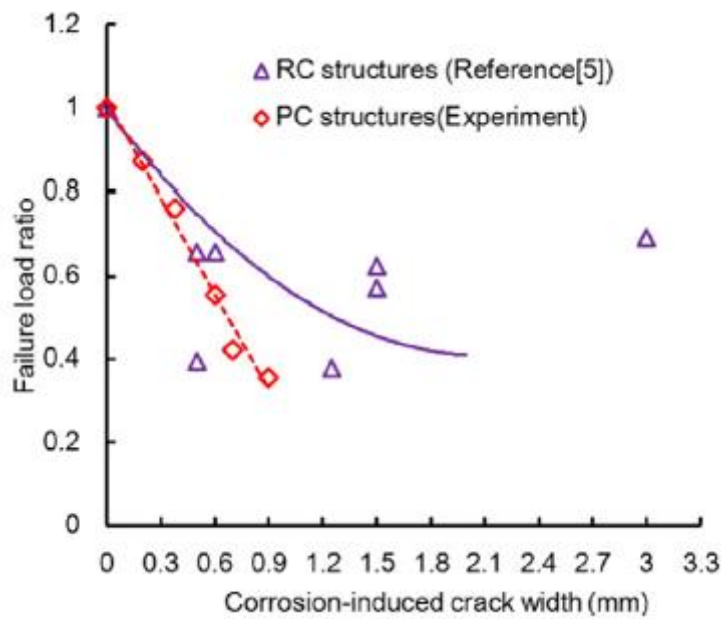


Figure 4.6 Failure load of specimens [4]

The comparison in figure 4.7 between experimental and theoretical results shows that the observed results were slightly higher than the predicted widths with an average error of 10.4%.

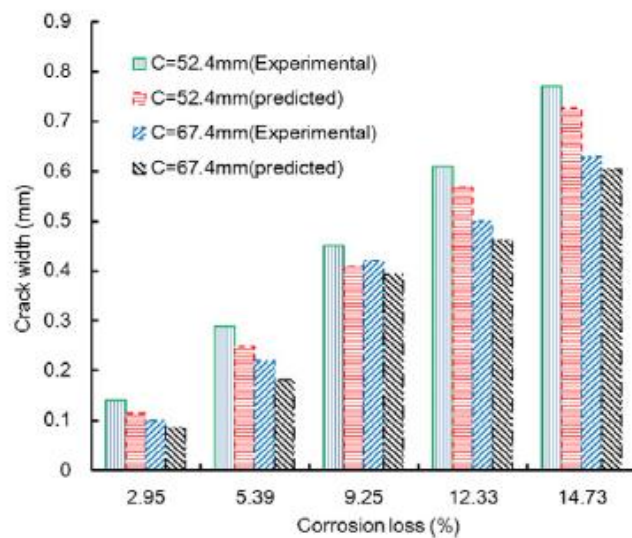


Figure 4.7 The experimental and predicted crack widths [4]

The predicted errors are acceptable in view of the complexity of the corrosion process, the theoretical errors may be attributed to the measurement uncertainty of crack width and corrosion loss, moreover the heterogeneity and variability of materials might have affected the prediction.

In conclusion is important to say that corrosion-induced crack increases significantly the risk of beam failure and this failure load degradation caused by corrosion induced cracking is more significant in PC structures than that in RC structures.

Prestress has an adverse effect on corrosion-induced cracking in PC structures and the decrement of critical corrosion loss becomes more important at the three stages.

4.2. The effect of stirrups on the filling of corrosion products and concrete cracking

A relevant aspect in the corrosion induced cracking is the presence of stirrups which affect both the filling of rust and concrete cracking. Wang et al. (2016), proposed the concrete cracking prediction including the filling proportion of strand corrosion products.

4.2.1. Specimens details and accelerated corrosion of strand

Two groups of samples were considered: group RS with stirrups and group S without stirrups. In total twelve specimens were designed with a square cross-section of 150 mm x 150 mm, and 1200 mm in length, as shown in the figure 4.8.

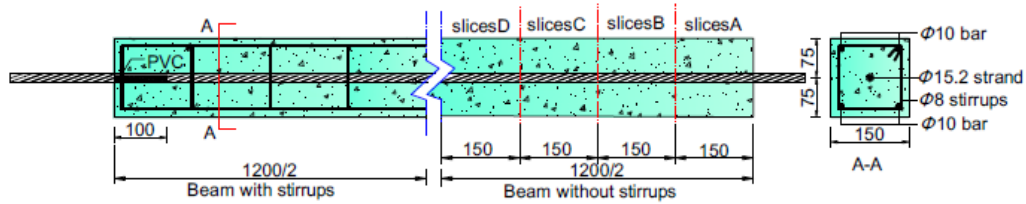


Figure 4.8 Details of the beam [mm] [5]

The test specimens were immersed in the saline solution for three days before the accelerated corrosion, then the specimens were immersed in the 5% sodium chloride (NaCl) solution in a designed tank.

The corrosion system consisted of a direct current potentiostat and a stainless-steel plate. The strand acted as the anode, and the stainless-steel plate served as the cathode. The direct current flowed from the positive terminals of the potentiostat to the strand, and then through saturated concrete and saline solution to the stainless-steel plate, and finally back to the negative terminals of the potentiostat.

Moreover, accelerated corrosion times have been obtained for all the samples and crack width and corrosion loss were measured, as shown in the table 3.

Beams	Corrosion time (days)
S	2
S	9
S	7
S	3
S	5
S	6
RS	7
RS	8
RS	14
RS	9
RS	3
RS	3

Table 3 Accelerated time of specimens [5]

4.2.2. Prediction Model of Crack Propagation

The thick-walled cylinder model, as shown in the figure 4.9, was used to predict the crack propagation based on corrosion loss.

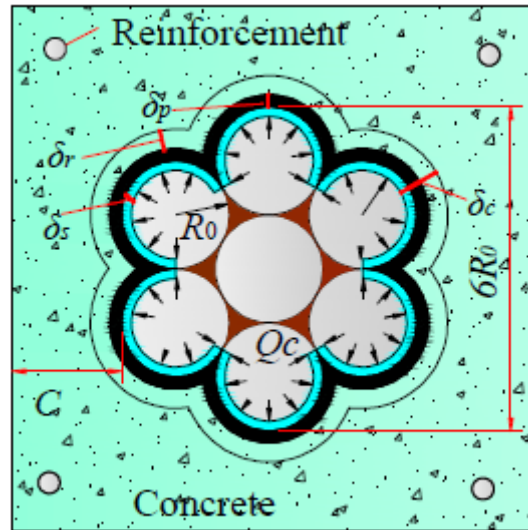


Figure 4.9 Expansive deformation at the strand-concrete interface (micro crack formation) [5]

The filling of corrosion products and geometric properties of the strand are incorporated in the model. During the corrosion process, corrosion products first fill the pores around the strand-concrete interface and then contribute to the expansive pressure. After that, it would fill the corrosion-induced cracks. With the principle of volume equal to the corrosion products, the relationship between the crack width and corrosion loss can be obtained. The micro-crack forms when the tangential stress exceeds the concrete tensile strength.

The tangential stress is derived with an elastic mechanics axisymmetric stress solution. Then, the maximum expansive pressure at the micro-crack formation can be obtained.

$$Q_{cmax} = \left(0.225 + 0.075 * \frac{C}{R_0}\right) * f_t \quad (4.9)$$

where f_t is the concrete tensile strength;

C is the concrete cover;

R_0 is the radius of the wire.

Finally, the volume of corrosion products at the micro-crack formation is calculated as:

$$V_m = \frac{\pi n R_0}{(n-1)E_c} \left[\left(0.9 + 0.3 \frac{C}{R_0} \right) f_t (1 + k + \nu_c) (R_0 + \delta_p) + E_c \delta_p \right] \quad (4.10)$$

where:

n is the rust expansion ratio;

E_c is the elastic modulus of concrete;

k is a constant

$$k = \frac{2(R_0 + \delta_p)^2}{C^2 + 2C(R_0 + \delta_p)} \quad (4.11)$$

ν_c is the Poisson's ratio of concrete;

δ_p is the thickness of the porous zone.

Therefore, after cover cracking cracks width can be observed and a trapezoid model can be proposed, as shown in the figure 4.10:

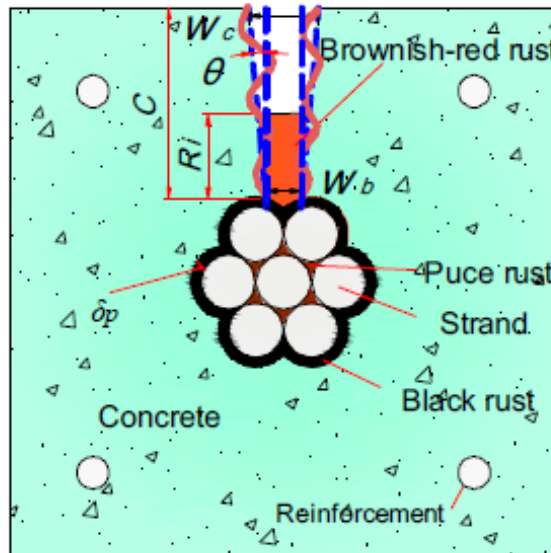


Figure 4.10 Simplified crack model [5]

For simplicity the corrosion products were considered in the wider opening and the smaller cracks were neglected.

As observed in the previous experiment, the filling of corrosion products varies with increasing crack width so the volume of corrosion products in the cracks can be written as:

$$V_p = [w_c + C(f - 2)\tan\theta]xR_i \quad (4.12)$$

where

- f the rust filling ratio equal to R_i/C
- R_i the average rust filling depth;
- θ is the cracking angle;
- w_c in the crack width on the concrete surface.

With the equal principle of volume, the total volume of corrosion products

$V_c = V_m + V_p$ and the crack width on the concrete surface is:

$$w_c = C(f - 2)(b - a\rho) + \frac{nV_s\rho}{Cf} - \frac{\pi nR_0 \left[\left(0.9 + 0.3\frac{C}{R_0}\right) f_t(1 + k + \nu_c)(R_0 + \delta_p) + E_c\delta_p \right]}{(n - 1)E_c C f} \quad (4.13)$$

where a and b are constants that depend on the presence or absence of stirrups;

ρ is the corrosion loss of the strand;

V_s is the strand volume per units of length and is equal to:

$$V_s = \frac{V_c}{n\rho} \quad (4.14)$$

4.2.3. Conclusions

Figure 4.11 shows the linear regression and polynomial regression of rust-filling ratio and crack width. It is clear that the rust-filling ratio increases faster in the specimens with stirrups than that in the specimens without stirrups.

In conclusions thanks to experimental test and theoretical analysis:

Using stirrups can decrease the critical crack width because stirrups can restrict the corrosion induced crack propagation, as shown in the 4.11.

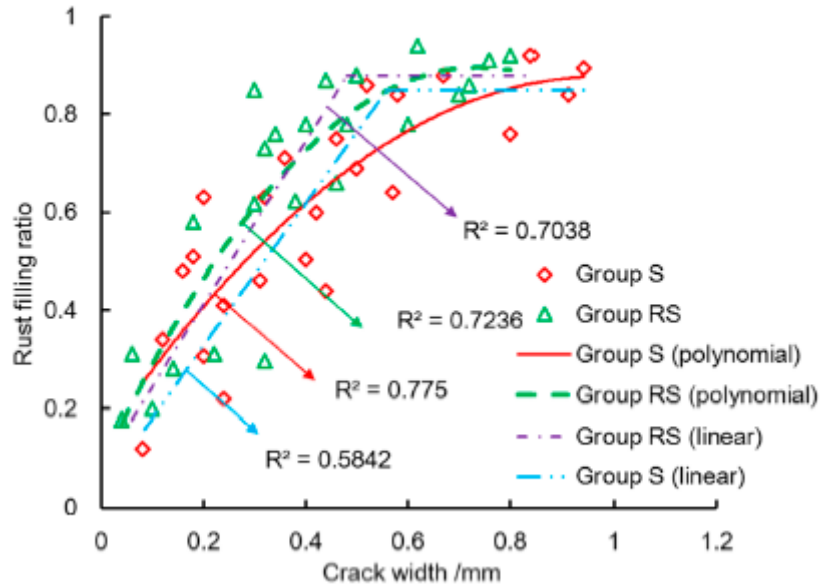


Figure 4.11 Rust filling ratio and crack width [5]

Finally, the proposed model can provide a reasonable prediction for corrosion-induced crack width and these predictions are sensitive to the rust filling extent.

5. Concrete cracking prediction under combined prestress and strand corrosion

A deep study related to the associated effects of precompression and corrosion of strand was performed by Wang et al. (2019). The analytical model was also tested by an experimental campaign considering four levels of prestressing and specimens subjected to accelerated artificial corrosion.

5.1. Experimental program

Tables 4 and 5 show the chemical composition and the mechanical characteristic of the steel (Li at al., 2011), while figure 5.1 describe the characteristic of the beam.

Type	Fe	C	Mn	Si	P	S	Cr	Cu	Ni	Ti	Al
Strand	97.862	0.82	0.74	0.21	0.012	0.006	0.17	0.09	0.03	0.03	0.03
Reinforcement	97.849	0.2	1.34	0.55	0.033	0.028	-	-	-	-	-

Table 4 Chemical composition of steel [1]

Type	Diameter(mm)	Yeld strength (MPa)	Ultimate strength (MPa)	Elastic modulus (GPa)
Strand	15.2	1830	1910	195
Deformed bars	6(8)	400	540	200

Table 5 Mechanical characteristic of steel [1]

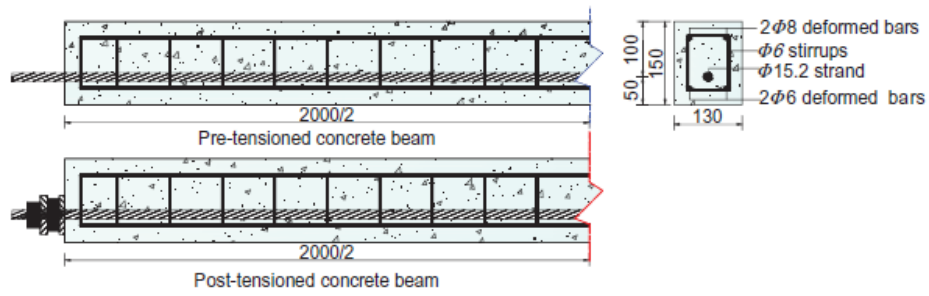


Figure 5.1 Details of the beams [mm] [1]

The specimens were divided into three groups A, B and C depending on the corrosion time and the type of prestressing to which the samples are subjected.

Type of beam	Corrosion time [days]
Group A pre-tensioned concrete	15
Group B Pre-tensioned concrete	20
Group C Post-tensioned concrete	20

Table 6 Type of beam [1]

Overall are twelve beams with a rectangular cross section of base equal to 130mm, 150mm of height and 2000mm in length. A 15.2mm diameter seven-wire steel strand with concrete cover of 42.4mm was used in this study's analysis, and four deformed bars of HRB400 with concrete cover of 30.0mm were employed as the hanger bars in the beam. Stirrups used in the beam have a 6mm diameter and 100mm spacing. Characteristics of the cement used are the following: Type 32.5

Portland cement and the concrete mix contained: 417 kg/m³ cement, 676 kg/m³ fine aggregates and 1026 kg/m³ rough aggregates. The water-cement ratio of concrete was 0.44.

Considering an ultimate strength f_p of 1860 Mpa, four levels of prestressing equal to 0, 0.25 f_p , 0.5 f_p and 0.75 f_p were assessed. The pre-tensioned and post-tensioned concrete beams were cast separately. The 28-day uniaxial compressive strengths of pre-tensioned and post-tensioned concrete were 44.1 and 43.4 MPa, respectively. The corrosion device, showed in Figure 5.2, was used to corrode the strand



Figure 5.2 Accelerated corrosion device [1]

The reinforcement was protected by epoxy resin; the strand was connected to the anode and the stainless-steel plate dipped in 10% NaCl was used as a cathode. In the present test all beams were subjected to the same corrosion current density of approximately 90 $\mu\text{A}/\text{cm}^2$.

After the accelerated corrosion the samples were broken, the corroded strands were removed, and the corrosion products were collected and dried with a baking box. Using the planetary ball mill, corrosion products have been reduced to dust. Later, the compositions of the corrosion products were measured using infrared Spectroscopy (IR) and thermal gravimetry (TG). IR spectroscopy was performed

using a Nicolet 6700 FTIR spectrometer. TG, with a heating rate of 10 C / min from 36 to 1000 C, was conducted on a DTG-60H thermal analyser.

After the accelerated corrosion, crack widths in the longitudinal direction were measured every 10 cm by a portable microscope with a resolution of 0.01mm. After removing the corroded strand from the concrete, the corrosion products on the surface of the wire were cleaned with 12% hydrochloric acid solution, then the wire was neutralized with alkali (ASTM. G1-03, 2011). Subsequently, the wire was cut into 10 cm in length and the loss of mass was measured.

5.2. Experimental results and discussion

Table 7, figure 5.3 and figure 5.4 shows the experimental results; three main considerations can be done:

- The critical time of the cover cracking is lowered by increasing the level of prestressing;
- Crack width in pre-tensioned beams is usually larger than post-tensioned beams under the same corrosion time. Moreover, varying prestress from 0 to 0.75fp, the maximum crack widths in groups A, B and C increase by 19%, 30% and 30%, respectively.
- Prestressing can accelerate the rate of crack propagation. When the prestressing level is zero, a corrosion loss of 10% can induce a crack width of 0.76 mm, at the other three prestressing levels the crack width increases by 3%, 7% and 11% respectively.

By varying the prestressing level from 0 to 0.75fp the propagation rate increases by 9%, therefore the four curves differ slightly and are almost superimposed.

Beam no./prestress	PA0/0	PA1/0.25fp	PA2/0.50fp	PA3/0.75fp	PB0/0	PB1/0.25fp	PB2/0.50fp
Critical time of cover cracking (h)	149	147	125	121	154	146	132
Critical time decrement (%)	NA	1	16	19	NA	5	14

Beam no./prestress	PB3/0.75fp	PC0/0	PC1/0.25fp	PC2/0.50fp	PC3/0.75fp
Critical time of cover cracking (h)	112	175	162	150	138
Critical time decrement (%)	27	NA	7	14	21

Table 7 Critical time of cover cracking [1]

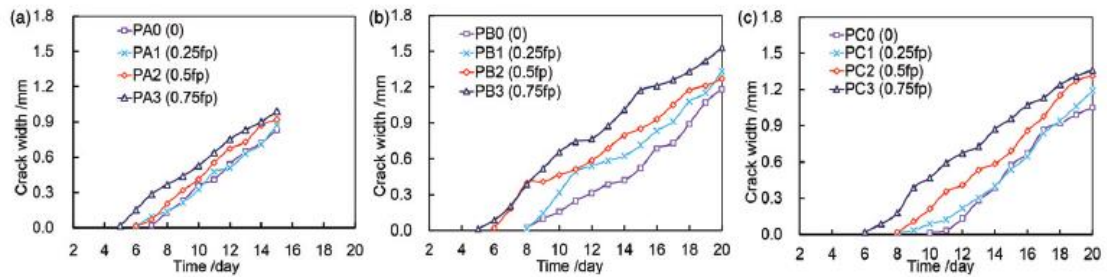


Figure 5.3 Crack propagation over time for groups A,B and C [1]

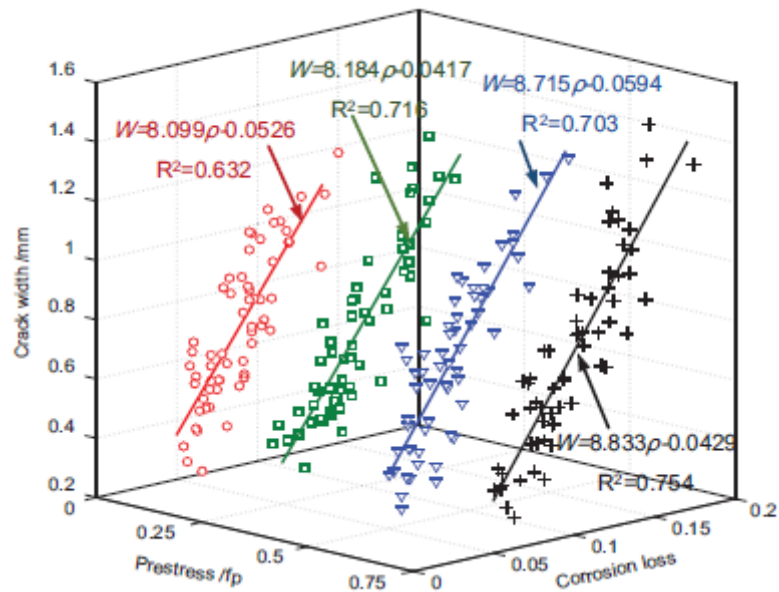


Figure 5.4 Crack widths and corrosion losses under various prestress [1]

5.3. Analytical model to predict the PC cracking from initiation to propagation

Since concrete is a heterogeneous material, a porous zone surrounds the strand-concrete interface. Corrosion products first diffuse into the porous zone, as corrosion products exceed the quantity needed to fill the porous zone, these products generate expansive pressure. When the tensile stress induced by expansive pressure exceeds the concrete tensile strength, concrete is considered to crack.

Figure 5.5 shows the stress distribution at the strand-concrete interface.

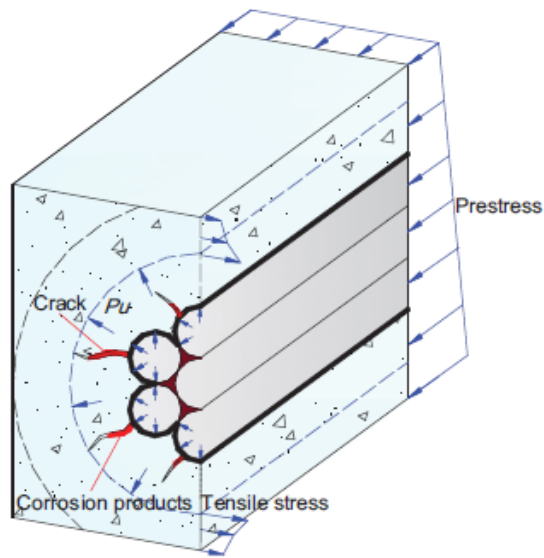


Figure 5.5 Stress distribution around the strand-concrete interface in PC beams [1]

In the present model the thick-walled cylinder theory is used, and a seven-wire steel strand was selected as an object of analysis. This strand was chosen because it is a very frequent situation in prestressed beams. It can be seen in figure 29 that the contact area of the outer wire is equal to two-thirds of the surface area (Lizhao Dai, Lei Wang, Jianren Zhang, Xuhui Zhang, 2016).

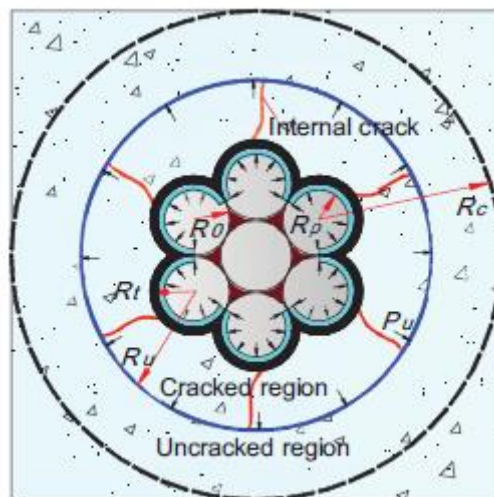


Figure 5.6 Concrete cracking due to strand corrosion [1]

In general, during the corrosion process of the entire strand the external wires will be the first to be corroded, moreover the corrosion loss of strand is equal to:

$$\rho = 4\pi(R_0^2 - R_\rho^2)/A_p \quad (5.1)$$

Where

A_p is the strand cross-sectional area (139 mm² from present study);

R_0 is the radius of wire before corrosion;

R_ρ is the radius of wire after corrosion.

During the corrosion process and the production of rust product, not all of them contribute to the pressure build up, but an amount would fill pores and cracks. Therefore, for the principle of conservation of the volumes the total volume of the corrosion products of the strand is given by the sum of three contributions:

$$\Delta v_r = \Delta v_w + \Delta v_c + \Delta v_p \quad (5.2)$$

where $\Delta v_r = n\Delta v_w$;

n is the rust expansion ratio and a value of 2.78 was considered. The experimental data in the table 8 show a range that varies from 2.68 to 2.96 considering the four levels of prestressing. Varying the prestressing the effect on n is minimal so an average value was taken.

Prestress (Mpa)	Weight loss at 200–400°C (%)	Mass percentage of iron hydroxide (%)	Mass percentage of iron oxide (%)	Rust expansion ratio
0	7	69	31	2.96
0.25 f_p	4	40	60	2.68
0.5 f_p	4	40	60	2.68
0.75 f_p	5	49	51	2.78
Average rust expansion ratio				2.78

Table 8 Parameters of corrosion products [1]

Δv_w is the volume change of wires and is equal to:

$$\Delta v_w = \frac{2}{3}\pi(R_0^2 - R_\rho^2) \quad (5.3)$$

Δv_c is the volume change of concrete induced by expansive pressure and is equal to:

$$\Delta v_c = \frac{2}{3}\pi(R_t^2 - R_0^2) \quad (5.4)$$

with R_t the radius of wire with corrosion products;

Δv_p is the volume of corrosion products that fill cracks and pores.

Δv_w and Δv_c can be derived from the geometric considerations mentioned above on the contact area of the external wires.

Δv_p can be obtained by referring to the article “modelling cover-cracking due to reinforcement corrosion in RC structures” written by S.J. Pantazopoulou and K.D. Papoulia. In the article mentioned above, the volume of corrosion products is obtained as the sum of two contributions: the first relates to corrosion products that generate pressure, while the second relates to the corrosion products that fill the openings and it is this second contribution that is derived from the article. The total space available within cracks is approximated as $\sum w(R_u - R_t)/2$, therefore:

$$\Delta v_p = \pi * u_r * (R_u - R_t) \quad (5.5)$$

Where u_r is calculated in R_0 and is equal to $(R_t - R_0)$ and R_u is the radius of the cracked region. The displacement to the strand-concrete interface is calculated by combining the equations 4.15 - 4.19:

$$u_c = R_t - R_0 = \frac{(n - 1) * A_p * \rho}{4\pi(R_u + R_0)} \quad (5.6)$$

With the introduction of prestressing, the following consequences are considered:

- The concrete is subject to a biaxial stress state expressed by the following equation (Tasuji, Slate, & Nilson, 1978)

$$\frac{\sigma_p}{f_{ck}} = \frac{1}{1 + KS} \quad (5.7)$$

where

σ_p is the compressive stress of concrete at the strand location;

$$K = \frac{f_t}{\sigma_p};$$

f_t is the concrete tensile strength under the biaxial stress state;

$$S = \frac{f_{ck}}{f_{tk}};$$

f_{ck} is the uniaxial compressive strength of concrete (equal to 44.1 pre-tensioned concrete);

f_{tk} is the uniaxial tensile strength of concrete;

Moreover, from the following equation can be obtained the compressive stress of concrete induced by the prestress $\sigma(y)$:

$$\sigma(y) = \frac{N_p}{A} + \frac{N_p e_p}{I} y \quad (5.8)$$

with

N_p the prestressing force of strand;

A the cross-sectional area of concrete;

e_p the eccentricity of strand;

y the distance from the position of concrete to the section centroid of concrete;

I the moment of inertia of concrete cross-section.

Combining equations 5.7 and 5.8 and approximating e_p equal to y , f_t is :

$$f_t = (f_{ck} - \sigma_p) * \left(\frac{f_{tk}}{f_{ck}}\right) \quad (5.9)$$

- Prestress can accelerate the corrosion-induced cracking process

To take into account the anisotropic behaviour of cracked concrete, a tangential stiffness reduction factor a (<1) can be derived from the concept of fracture energy, as shown in the figure 5.7.

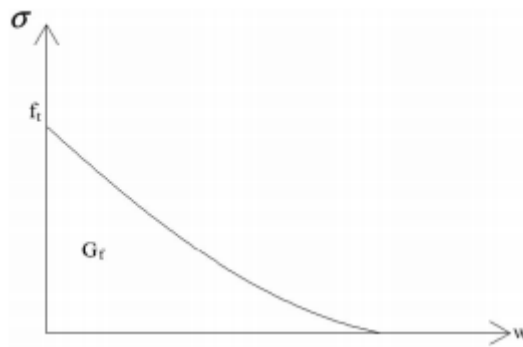


Figure 5.7 Postcrack stress and crack width relationship (data from Shah et al. 1995)

In figure 5.7 the initial condition is $\sigma(0) = f_t$ = tensile strength of concrete, instead

$$G_t = \int_0^w \sigma(w)dw.$$

Therefore, the factor is considered as (Li & Yang,2011)

$$a = \frac{f_t \exp(-\lambda(\bar{\varepsilon}_\theta - \bar{\varepsilon}_\theta^c))}{\bar{\varepsilon}_\theta E_c} \quad (5.10)$$

where

$$\lambda = \pi \frac{f_t}{G_t} (R_0 + R_u);$$

G_t is the fracture energy (0,088 from Li and Yang,2011);

$\overline{\varepsilon_\theta}$ is the average residual tangential strain of cracked concrete;

$\overline{\varepsilon_\theta^c}$ is the average tangential strain of uncracked concrete;

E_c is the elastic modulus of concrete (32500 MPa from MHURD, 2010).

It is assumed for simplicity that a is constant, which means that the residual tangential strain $\overline{\varepsilon_\theta}$ and $\overline{\varepsilon_\theta^c}$ are average values (C.Q. Li and S.T. Yang).

The radial and tangential stresses of cracked concrete are:

$$\sigma_r(r) = \frac{E_c}{1 - \nu_c^2} \left(\varepsilon_r(r) + \nu_c \sqrt{a} \varepsilon_\theta(r) \right) \quad (5.11)$$

$$\sigma_\theta(r) = \frac{E_c}{1 - \nu_c^2} \left(a \varepsilon_\theta(r) + \nu_c \sqrt{a} \varepsilon_r(r) \right) \quad (5.12)$$

Where

$R_0 < r < R_u$ is the radius of concrete at the cracked region;

$\varepsilon_r(r) = \frac{\pi du(r)}{dr}$ are the radial strains of concrete

$\varepsilon_\theta(r) = \frac{u(r)}{r}$ are the tangential strains of concrete;

In the cracked region $\nu_c = \sqrt{\nu_1 \nu_2}$, in fact there are two different Poisson's ratios in the tangential and radial direction (Li & Yang 2011) ν_1 and ν_2 . In this model a value of 0.18 was considered for ν_c , referring to Liu and Weyers,1998.

For the cracked region, the concrete stress in the radial direction should satisfy the following equilibrium equation:

$$\frac{\partial \sigma_r(r)}{\partial r} + \frac{\sigma_r(r) - \sigma_\theta(r)}{r} = 0 \quad (5.13)$$

The governing equation for the displacement in the cracked concrete cylinder is equal to:

$$\frac{d^2 u(r)}{dr^2} + \frac{1}{r} \frac{du(r)}{dr} - a \frac{u(r)}{r^2} = 0 \quad (5.14)$$

Considering two unknown parameters to be calculated later, it is possible to obtain the displacement in the cracked region

$$u(r) = b_1(r)r^{\sqrt{a}} + b_2(r)r^{-\sqrt{a}} \quad (5.15)$$

To calculate the radial and tangential stresses of cracked concrete it is possible to combine the equations 5.11, 5.12 and 5.15 therefore:

$$\sigma_r(r) = \frac{\sqrt{a}E_c}{1 - \nu_c^2} [b_1(r)(1 + \nu_c)r^{\sqrt{a}-1} - b_2(r)(1 - \nu_c)r^{-\sqrt{a}-1}] \quad (5.16)$$

$$\sigma_\theta(r) = \frac{aE_c}{1 - \nu_c^2} [b_1(r)(1 + \nu_c)r^{\sqrt{a}-1} + b_2(r)(1 - \nu_c)r^{-\sqrt{a}-1}] \quad (5.17)$$

On the other hand, tensions and displacement in the uncracked region can be derived from the elasticity theory considering:

$$R_u < t < R_c;$$

$$R_c = R_0 + C;$$

C the concrete cover (42.4 mm from present study);

P_u the expansive pressure at the interface between the cracked and uncracked regions.

$$\sigma_r(t) = \frac{R_u^2 P_u}{(R_c^2 - R_u^2)} \left(1 - \frac{R_c^2}{t^2} \right) \quad (5.18)$$

$$\sigma_\theta(t) = \frac{R_u^2 P_u}{(R_c^2 - R_u^2)} \left(1 + \frac{R_c^2}{t^2} \right) \quad (5.19)$$

$$u(t) = \frac{(1 + \nu_c) R_u^2 P_u}{E_c (R_c^2 - R_u^2)} \left[\frac{R_c^2}{t} + (1 - 2\nu_c) t \right] \quad (5.20)$$

At the interface between the cracked and the uncracked region the following boundary conditions are valid:

- the condition of equality between the tensile stress and the concrete tensile strength $\sigma_\theta(R_u) = f_t$, therefore the expansive pressure at the interface is equal to:

$$P_u = f_t \frac{R_c^2 - R_u^2}{R_c^2 + R_u^2} \quad (5.21)$$

- two conditions related to radial stress and deformation $u(t) = u(r)$ and $\sigma_r(t) = \sigma_r(r)$.

Therefore considering the parameter $m = \frac{(1+\nu_c)f_t}{E_c(R_c^2+R_u^2)} [R_c^2 + (1-2\nu_c)R_u^2]$ it is possible to obtain the two unknown parameters $b_1(r)$ and $b_2(r)$

$$b_1(r) = \frac{(1 - \nu_c)m + P_u(1 - \nu_c^2)/\sqrt{a}E_c}{2R_u^{\sqrt{a}-1}} \quad (5.22)$$

$$b_2(r) = \frac{(1 + \nu_c)m + P_u(1 - \nu_c^2)/\sqrt{a}E_c}{2R_u^{-\sqrt{a}-1}} \quad (5.23)$$

To calculate the reduction factor a , it is necessary to make explicit the values of the average tangential strain of uncracked and cracked concrete: $\overline{\varepsilon_\theta^c}$ and $\overline{\varepsilon_\theta}$

$$\overline{\varepsilon_\theta^c} = \frac{1}{R_u - R_0} \int_{R_0}^{R_u} \frac{u(t)}{t} dt \quad (5.24)$$

$$\overline{\varepsilon_\theta} = \frac{1}{R_u - R_0} \int_{R_0}^{R_u} \frac{u(r)}{r} dr \quad (5.25)$$

After determining the factor a , the corrosion loss of strand can be determined by combining equations 4.20 and 4.29

$$\rho = \frac{4\pi(R_u + R_0)[b_1(R_t)R_t^{\sqrt{a}} + b_2(R_t)R_t^{-\sqrt{a}}]}{(n - 1)A_p} \quad (5.26)$$

When $R_u = R_c$, as shown in the figure 5.8, i.e. in the condition of propagation of crack to the concrete surface the boundary conditions change.

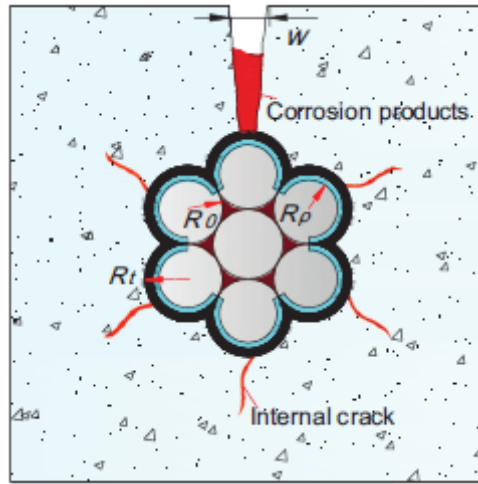


Figure 5.8 Crack propagation to the concrete surface [1]

The solution of equation 4.28 should be rewritten as

$$u(r) = b_3 r^{\sqrt{a}} + b_4 r^{-\sqrt{a}} \quad (5.27)$$

Where b_3 and b_4 can be derived from the new boundary conditions (Li et al.,2006)

$$b_3(1 + \nu_c)R_c^{(\sqrt{a}-1)} - b_4(1 - \nu_c)R_c^{(-\sqrt{a}-1)} = 0 \quad (5.28)$$

$$b_3 R_0^{\sqrt{a}} + b_4 R_0^{-\sqrt{a}} = R_t - R_0 \quad (5.29)$$

Therefore, it is possible to calculate the unknown parameters:

$$b_3 = \frac{(R_t - R_0)(1 - \nu_c)R_0^{\sqrt{a}}}{(1 + \nu_c)R_c^{2\sqrt{a}} + (1 - \nu_c)R_0^{2\sqrt{a}}} \quad (5.30)$$

$$b_4 = \frac{(R_t - R_0)(1 + \nu_c)R_c^{2\sqrt{a}}R_0^{\sqrt{a}}}{(1 + \nu_c)R_c^{2\sqrt{a}} + (1 - \nu_c)R_0^{2\sqrt{a}}} \quad (5.31)$$

It is possible to calculate crack width w_c on the concrete surface considering the tangential strain of concrete $\varepsilon_\theta(R_c)$:

$$w_c = 2\pi R_c \left[\varepsilon_\theta(R_c) - \frac{f_t}{E_c} \right] \quad (5.32)$$

The equation 4.46 can finally be rewritten combining with the 4.41 as (Li et al.,2006)

$$w_c = \frac{4\pi(R_t - R_0)}{(1 - \nu_c) \left(\frac{R_0}{R_c}\right)^{\sqrt{a}} + (1 + \nu_c) \left(\frac{R_c}{R_0}\right)^{\sqrt{a}}} - \frac{2\pi R_c f_t}{E_c} \quad (5.33)$$

Combining equations 4.20 and 4.47 the corrosion loss of strand is equal to

$$\rho = \frac{4\pi(R_0+R_t)}{(n-1)A_p} (b_3 R_t^{\sqrt{a}} + b_4 R_t^{-\sqrt{a}}) \quad (5.34)$$

5.4. Implementation of the analytical model and evaluation of the results

To implement the analytical model, was used the software MATLAB and adopting an iterative process, the final result was found.

The fundamental unknown parameter is represented by the tangential stiffness reduction factor α which in turn depends on the average value of the crack width:

$$\alpha = f(\bar{w}) = f(\bar{\varepsilon}_\theta, \bar{\varepsilon}_\theta^c) \quad (5.35)$$

When the crack reaches the surface of the concrete cover i.e. $R_u = R_c$, it is possible to consider two contributions of the concrete related to the elastic part and the cracked part.

Concerning the elastic contribution, it is necessary to calculate $\bar{\varepsilon}_\theta^c$ which depends on the parameters C_3 and C_4 . The boundary conditions in this case are:

- 1) $\sigma_\theta^e(r = R_c) = f_t$
- 2) $\sigma_r^e(r = R_c) = 0$

Where f_t is the concrete tensile strength under the biaxial stress state. Therefore, it is possible to calculate the parameters C_3 and C_4 . Instead the cracked area is characterized by the following boundary conditions from which it is possible to calculate the two parameters C_1 and C_2 therefore $\bar{\varepsilon}_\theta$:

- 3) $\sigma_r^c(r = R_c) = 0$
- 4) $u_c(r = R_0) = (R_t - R_0)$

Using an iterative procedure called for loops, the value of α was obtained. Finally, the critical value of R_t was calculated using condition 5) and again using for loops procedure in MATLAB:

- 5) $\sigma_\theta(r = R_c) = f_t$

R_ρ was obtained considering:

- penetration attack $x_{ave} = R_0 - R_\rho$;
- the contribution of the volumetric expansion coefficient in the area calculation: $\pi * (R_t^2 - R_\rho^2) = \alpha * (\pi * (R_0^2 - R_\rho^2))$

The final part of the code concerns the calculation of the crack width starting from the critical value of R_t and the calculation of the tangential tension $\sigma_\theta(r)$.

It is important to remember that the radius related to corrosion products that fill pores, which don't create pressure, has been deducted from R_t .

5.5. Comparison with the experimental results

The effectiveness of the model is firstly tested by a comparison with the experimental results obtained by Andrade et al. on small reinforced beams artificially corroded. Using strain gauges applied on the surface of the samples, it have been monitored: the amount of current, the loss of the cross section of the bar and the evolution of the crack width. Four specimens were considered (Figure 31), that differ in:

- Bar position;
- Concrete cover;
- Applied current to induce artificial corrosion.

In the experimental procedure were considered specimens with a rectangular cross-section of 15cm x 15cm and 38cm in length, an ordinary corrugated rebar 16 mm in diameter and an average value of tensile strength of 3.55 MPa.

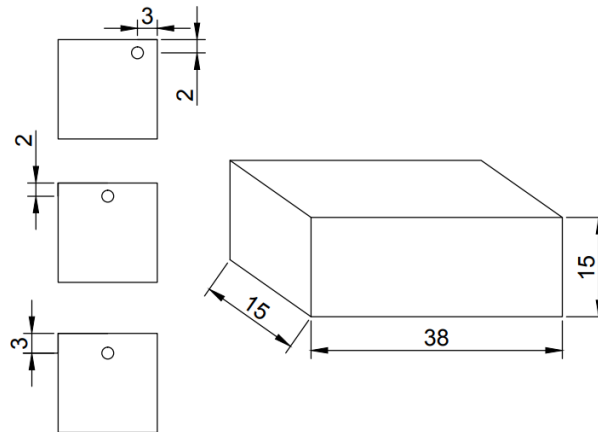


Figure 5.9 Type of reinforced concrete beam fabricated for the experimentation [7]

After being cured for 28 days, the samples were dried to glue the strain gauges. An ordinary potentiostat was used to apply a current of $100 \mu\text{A}/\text{cm}^2$ to the specimens I, II and III, while to the specimen IV a current of $10 \mu\text{A}/\text{cm}^2$ was applied, simulating

a more realistic and natural case. Based on the experimental results in the second part of the article a numerical model was proposed in which the following parameters were used:

- Volumetric expansion coefficient of two;
- Fracture energy of 200Jm^{-2} ;
- Elastic modulus of 36 GPa;
- Poisson's ratio of 0.2.

5.5.1. Results

Comparing the steel attack penetration and the cover maximum crack width in a figure 5.10 and 5.11, four curves relative to the four specimens analysed by Andrade et al. and, the curve that represents the analytical model developed in this thesis are compared.

Two different graphs were considered to distinguish the two cases of cover 20 and 30 mm.

It is clear that the model approximates the results of Andrade above all for steel attack penetration between 0.02 and 0.04 mm and therefore for relatively low values of corrosion.

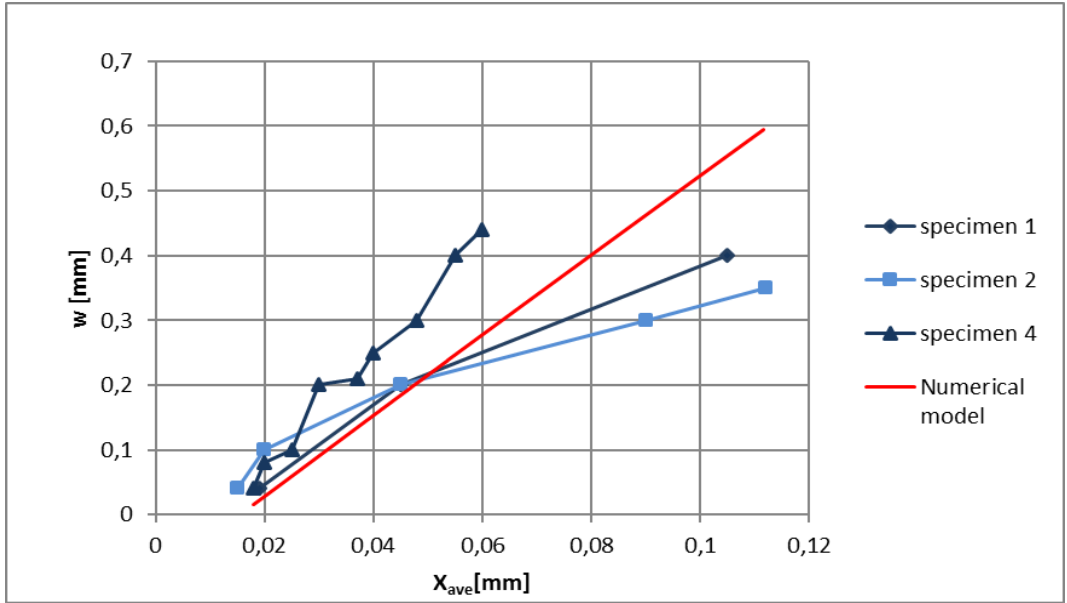


Figure 5.10 Loss in bar cross-section versus the crack width measured in the cover. Specimens with a concrete cover of 20 mm

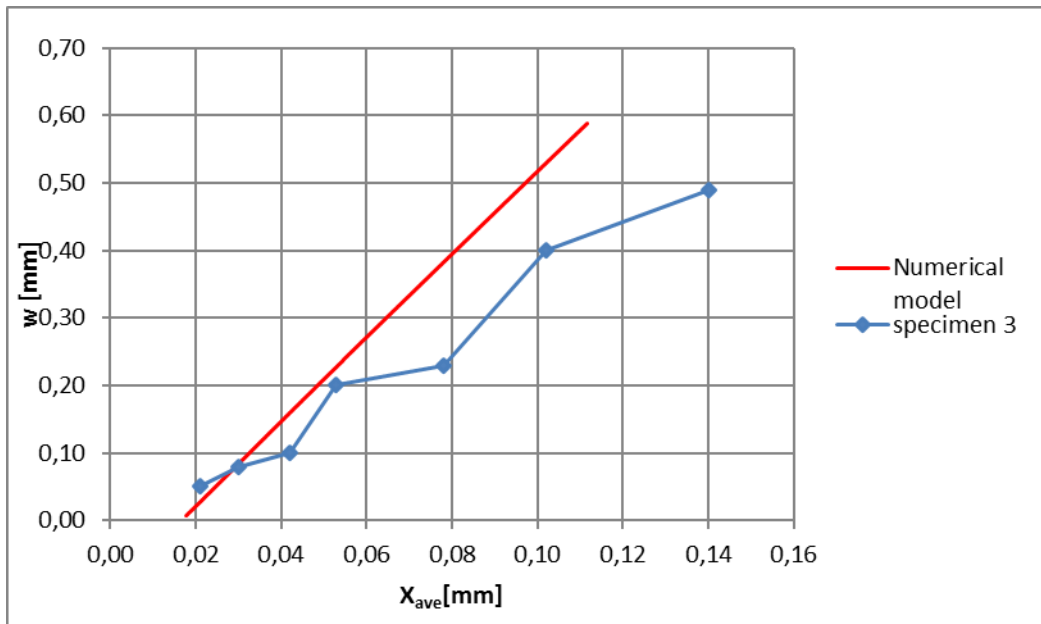


Figure 5.11 Loss in bar cross-section versus the crack width measured in the cover. Specimens with a concrete cover of 30 mm

It can be noticed that the model approximates the data relating to the first 3 specimens with a high corrosion rate, while for the IV specimen that has been artificially corroded with an intensity similar to natural corrosion, the curve of the model is more distant compared to the experimental data.

To detect this aspect, it is possible to vary the value of the volumetric expansion coefficient n in the analytical model.

It is evident that the model strongly depends on n and the rate of artificially induced corrosion: if the corrosion is slower the effect is more devastating because the oxides have time to hydrate and therefore are more expansive.

Therefore, as shown in the figure 5.12, Andrade's experimental data will overlap with the model at $n = 2.5$ and by increasing this coefficient the curves rise: at lower levels of corrosion correspond higher crack widths.

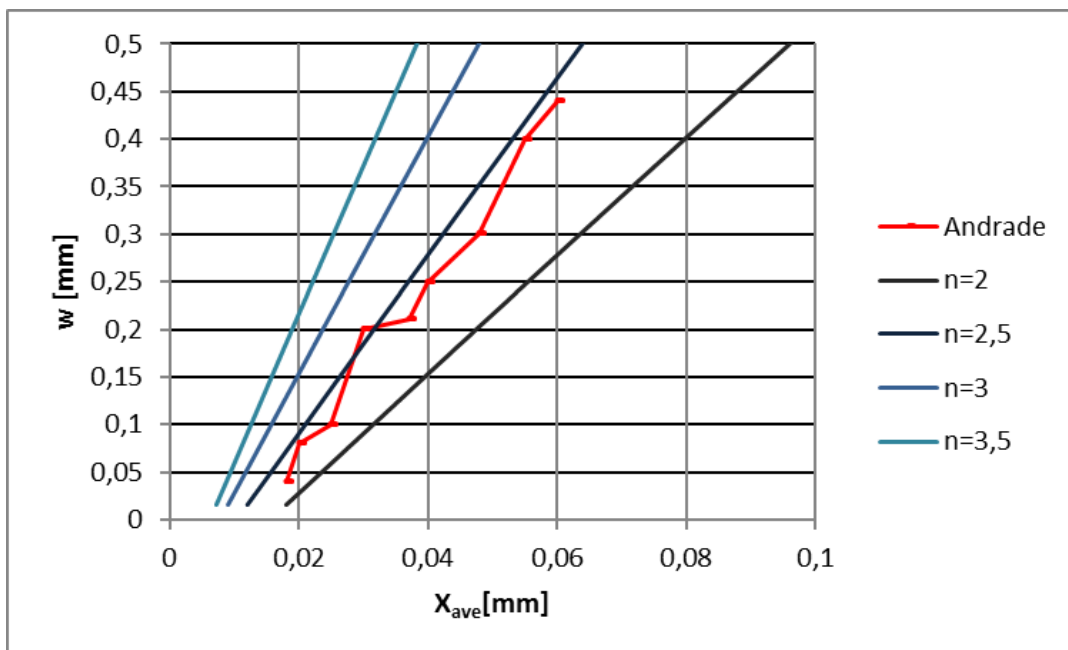


Figure 5.12 Evaluation of the analytical model by varying the volumetric expansion coefficient

5.6. Experimental results present in the literature and introduction of a new interpolation function

The phenomenon of corrosion can be divided into two phases: initiation and propagation time. The service limit state (SLS) and the ultimate limit state (ULS) of reinforced concrete structures are affected by the different effects caused by corrosion:

- reduction of the cross section;
- alteration of the bond;
- reduction of ductility and increase of embrittlement;
- concrete cracking, spalling and delamination of concrete cover;

The reduction of the transverse steel section can be uniform or localized depending on whether the corrosion is punctual or uniform. It is possible to calculate the reduced bar diameter knowing the corrosion attack depth P_x , the initial bar diameter and the coefficient of volumetric expansion α :

$$\varphi_{s,red} = \varphi_{s,ini} - \alpha P_x \quad (5.35)$$

Alonso et al. (10) established on the basis of 138 corroded samples, analysed by a linear regression model, a relationship between the penetration of corrosion and the openings of the cracks.

$$w = 0,05 + \beta(P_x - P_{x0}) \quad (5.36)$$

where:

- w is the crack width due to corrosion (smaller than 1 mm) [mm];
- β is a parameter depending on the bar position ($\beta=10$ for top cast bars and $\beta=12.5$ for bottom cast bars);
- P_x is the corrosion attack penetration [μm];

- P_{x0} is the corrosion attack penetration corresponding to the onset of the crack on the outer surface [μm].

For the calculation of P_{x0} it is possible to refer to two formulas present in literature written by Rodriguez and Alonso.

Rodriguez et al. (11)

$$P_{x0} = a + b_1 \frac{c}{\phi} - b_2 f_{ct} \quad (5.37)$$

where a and b are empirical coefficients whose values are shown in the table 9 and f_{ct} is the concrete tensile strength [MPa].

Parameter	Mean values	Characteristic values
a	74.5	83.8
b_1	7.3	7.4
b_2	-17.4	-22.6

Table 9 Empirical parameters for corrosion determination [6]

Alonso et al. (12)

$$P_{xo} = 7.53 + 9.32 \frac{c}{\phi} \quad (5.38)$$

where:

$\frac{c}{\phi}$ is the ratio between cover and bar diameter.

Finally, there is also a correlation between the crack opening with reinforcing bar corrosion:

Vidal et al. (13)

$$w = 0.0575(\Delta A_s - \Delta A_{s0}) \quad (5.39)$$

where:

ΔA_s is the section loss due to corrosion;

ΔA_{s0} is the section loss at the onset of the crack on the outer surface.

If ϕ_0 is the virgin radius of the reinforcing bar and α is the pit concentration factor, it is possible to make explicit ΔA_{s0} :

$$\Delta A_{s0} = A_s \left\{ 1 - \left[1 - \frac{\alpha}{\phi_0} \left(7.53 + 9.32 \frac{c}{\phi} \right) 10^{-3} \right]^2 \right\} \quad (5.40)$$

Most of the works for the evaluation of the crack width in the literature consider the $\frac{c}{\phi}$ ratio, in fact, assuming the same cover with the increase of the penetration of the corrosion, if the diameter of the bar is bigger, larger openings will be formed with respect to a bar of smaller diameter.

Other parameters such as the concrete tensile strength f_{ct} must be considered because greatly influences the beginning and propagation of cracks.

If the tensile strength of the concrete is greater, it is more likely that cracks due to the pressure of the oxides will be avoided, and once a crack appears, the more likely it is that its size will remain smaller than in the case of low concrete resistance.

The Table 10 shows some experiments in which the applied current density level was less than $200 \mu\text{A} / \text{cm}^2$.

Researches	J	f_{cm}	f_{ct}	c/Φ	load
	[$\mu\text{A}/\text{cm}^2$]	[MPa]	[MPa]	[-]	
Andrade et al. [4]	10-100	n/a	3.6	1.3, 1.9	n
Torres-Acosta and Martínez-Madrid [71]	Natural	n/a	1.9	1.9	n
Rodríguez et al. [57]	100	40.0	n/a	1.9 - 2.9	n
El Maaddawy et al. [28]	165	41.0	n/a	2.2	y/n
Torres-Acosta et al. [72]	80	27.0	2	2	n
Cairns et al. [13]	60	38.8	n/a	1.6, 2.6	n
Al-Harthy et al. [36]	59 - 169	23.8	8	0.4 - 1.3	n
Coronelli et al. [21]	143	34.3	n/a	1.5	n
Giordano et al. [33]	200	25.2	n/a	2.7	y
Richard et al. [56]	100	44.7	3.3	1.3	n
Prieto [53]	100 - 200	n/a	2 - 2.5	2.1, 3.4	n
Pull-out specimens	200	33.2	3.4	4.5	n

Table 10 Experimental test statistically analysed by the authors [14]

To consider the previous considerations, by introducing two parameters α and β determined to minimize data dispersion, a new parameter has been proposed by Cesetti (2017):

$$CT = \left(\alpha \frac{c}{\Phi} \right)^{-\frac{\beta}{f_{ct}}} \quad (5.41)$$

where c is the concrete cover;

Φ is the bar diameter;

f_{ct} is the average concrete tensile strength in MPa;

The values are 0.63 and 1.41 MPa for α and β respectively. It is possible to discover the interpolation curve for the selected data set, obtained by a linear regression using a power law as an interpolation function. The CT parameter is used as a multiplication factor for the $\frac{x_{ave}}{r_0}$ ratio, then

$$w_{max} = 15.863 * \left(\frac{x_{ave}}{r_0} * CT \right)^{0.928} \quad (5.42)$$

where w_{max} is expressed in mm.

The experimental data considered by means of upper and lower limit curves and the interpolation function are shown in a figure 5.13 on a logarithmic scale. The functions are obtained from a linear regression analysis corresponding to a 95% confidence interval.

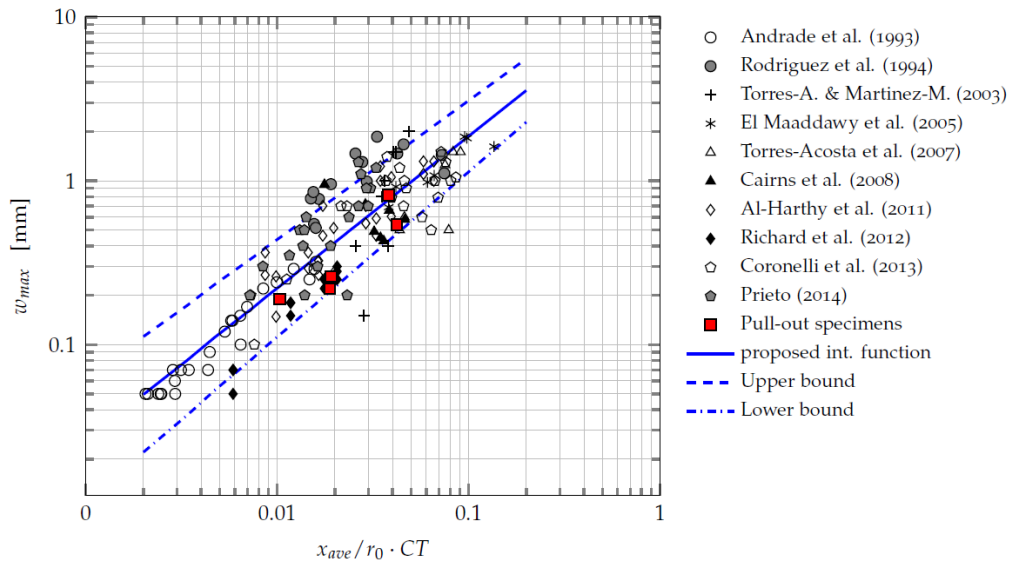


Figure 5.13 Crack widths as a function of normalized corrosion penetration for the modified collected data [6]

In conclusion, the Cesetti parameter CT has a general validity as, unlike most models that only consider the $\frac{c}{\phi}$ ratio, takes into account the various other factors that influence the cracks due to corrosion.

5.6.1. Comparison between the analytical model and experimental data present in literature

It is possible to do two checks related to the RC structures:

- A verification for the validity of the model studied is comparing the analytical model and the experimental data, always represented by two lower

and upper limits, an optimal positioning of the model within the curves can be seen in the figure 5.14.

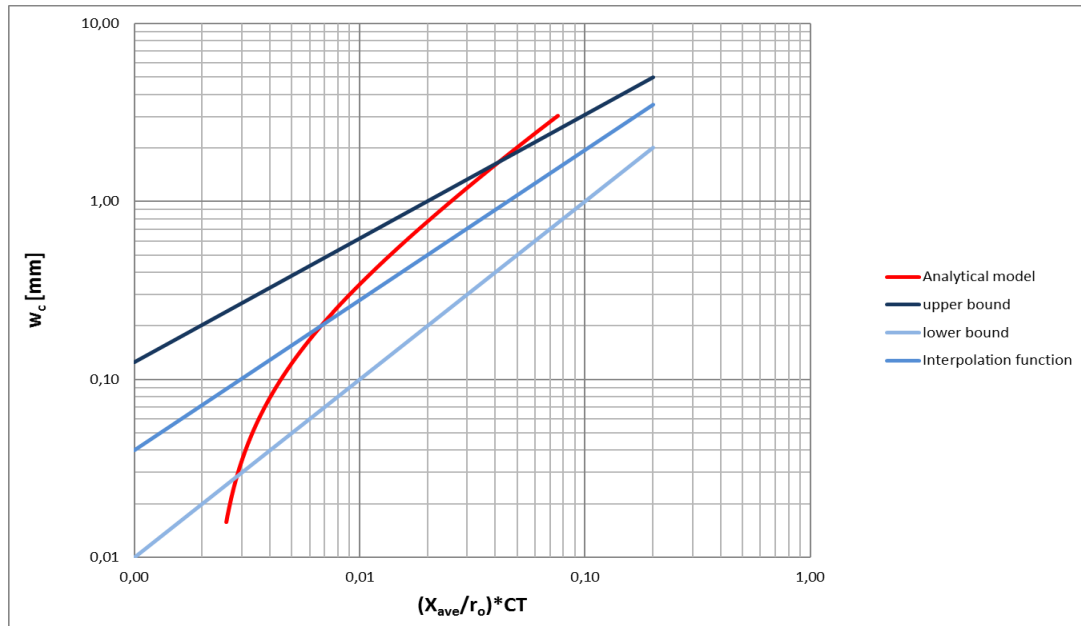


Figure 5.14 Validity of the analytical model studied

- A second comparison can be made by evaluating the experimental data relating to the IV specimen subject to an applied current of $10 \mu\text{A}/\text{cm}^2$ both with the interpolation function of Cesetti and with our studied analytical model. We get three curves in a graph crack width-attack penetration as shown in figure 5.15.

It is possible to note that, as already mentioned above, the model reflects well the results obtained with low penetration attack values.

Furthermore, at the penetration value of 0.035 mm the crack widths obtained with the Cesetti formulation are higher than the values obtained using the model, while from a penetration attack of about 0.04 mm the situation is reversed being the greater the slope of the curve of the model.

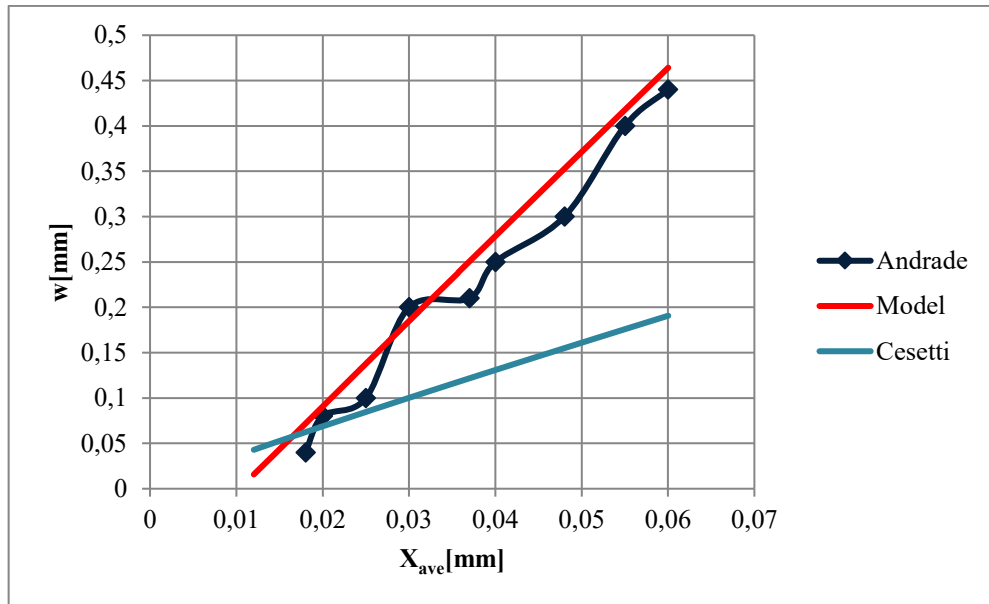


Figure 5.15 Evaluation of the analytical model with respect to Cesetti's experimental data

5.7. Application of the analytical model on corroded PC structures.

To evaluate the effects of prestressing on the crack width, the analytical model has been implemented considering different levels of prestressing and using the data already described in the theoretical treatment of the model.

Figure 5.16 and 5.17 show the comparison between the analytical model and the experimental data relating to the first and fourth prestressing levels.

It is clear that the model studied is more reliable closer to the cracking limit condition. This simplification of the model can be explained by the fact that the beneficial effect of the cover is considerable from the beginning of the crack propagation process until the openings reach the surface. It is also evident from the formula 5.33 that beyond the formation of the crack at the surface, the factor a tends to zero, so the effect of the concrete cover represented by R_c is lost.

According to the analytical model all the amount of oxide that is created makes the openings grow linearly. According to other studies, where the $\frac{C}{\phi}$ ratio is taken into account, in the assessment of crack width, other factors come into play such as:

- the possibility that the oxides created around the bar could make a greater path if there is a greater concrete cover;
- the possible dispersion of the oxides in the secondary cracks.

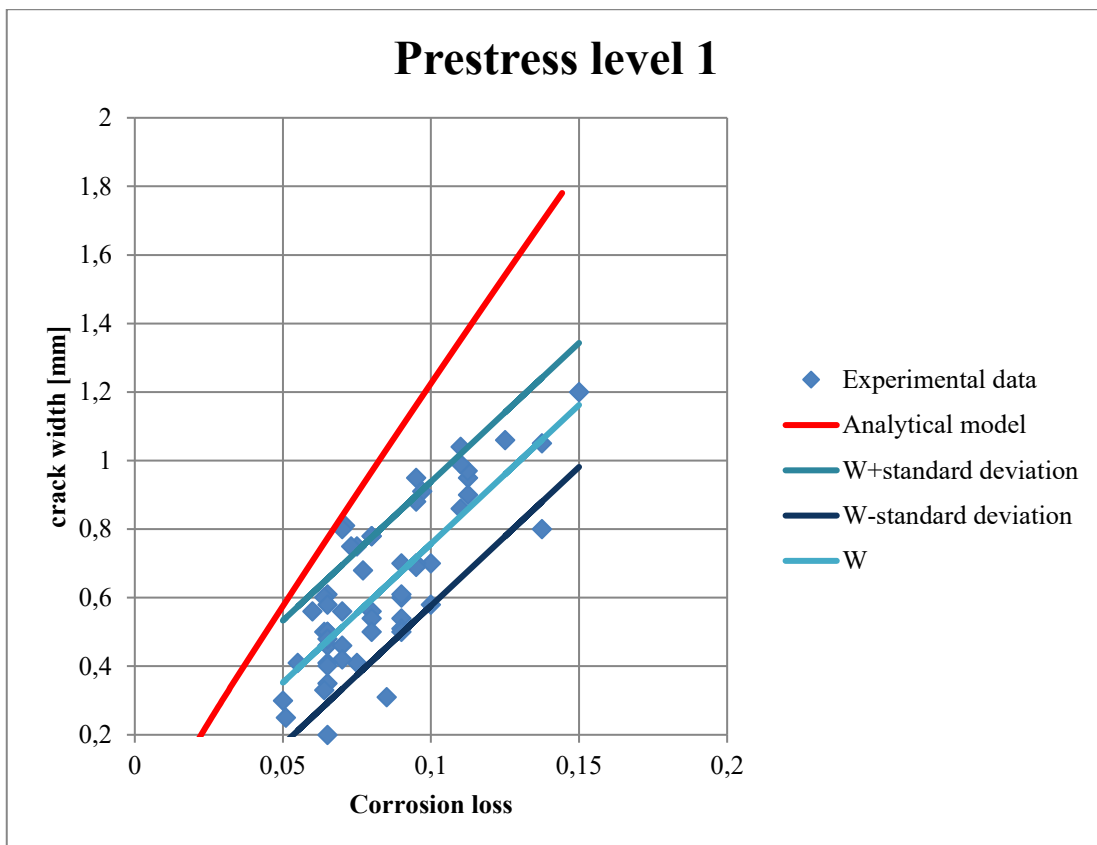


Figure 5.16 Comparison between experimental data and analytical model: first level of prestressing

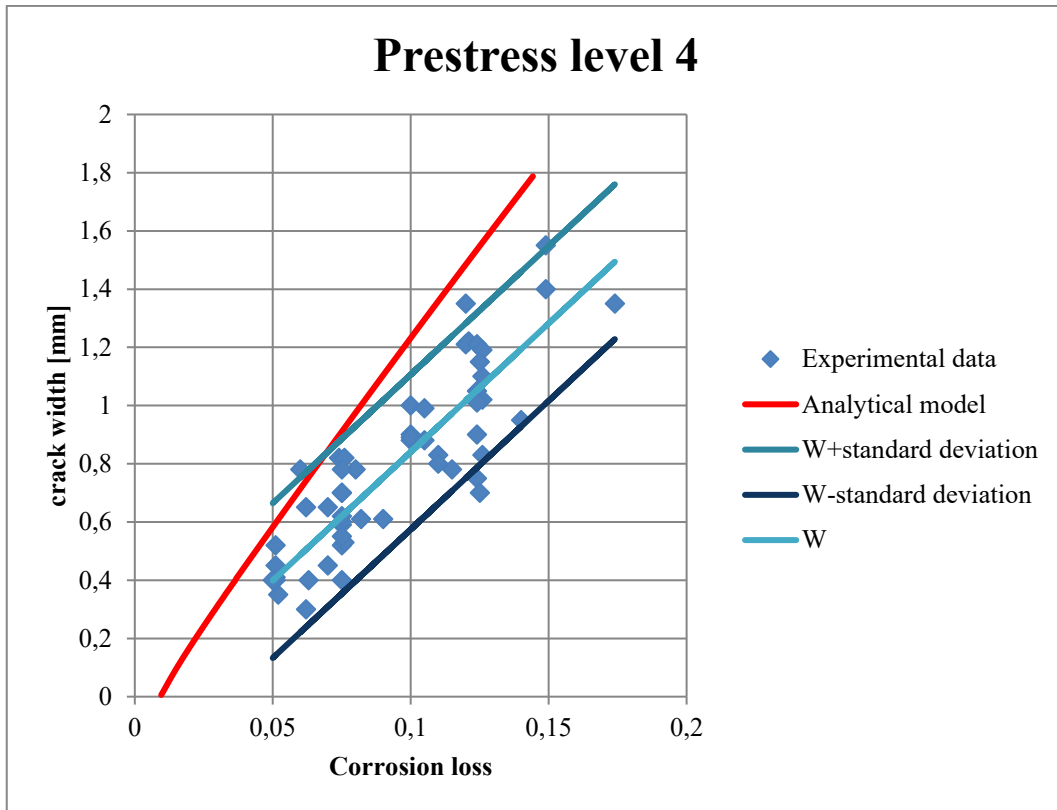


Figure 5.17 Comparison between experimental data and analytical model: fourth level of prestressing

5.7.1. Assessment of cracking time

The model studied, as already mentioned, is more reliable closer to the cracking condition. Therefore, it is possible to derive the level of critical corrosion starting from which there is the formation of the first crack.

In the study carried out by Andrade, discussed in paragraph 5.5, a formula is presented that links corrosion penetration and time elapsed since the propagation period began:

$$\phi(t) = \phi(i) - 0.023I_{corr} * t \quad (5.43)$$

where

$\phi(t)$ = rebar diameter (mm);

$\phi(i)$ = initial rebar diameter (mm);

I_{corr} = corrosion intensity ($\mu\text{A cm}^{-2}$);

0.023 = conversion factor ($\mu\text{A cm}^{-2}$ to mm for year).

The model was applied considering four different cases with different bar diameters. The same concrete cover was considered for the four cases and the same tensioning $\sigma_p = 1420$ MPa. Figures 5.18 and 5.19 show the critical values of the corrosion levels for each strand area. Using the 5.43, the time necessary for the cracking was obtained, after which the first crack was opened.

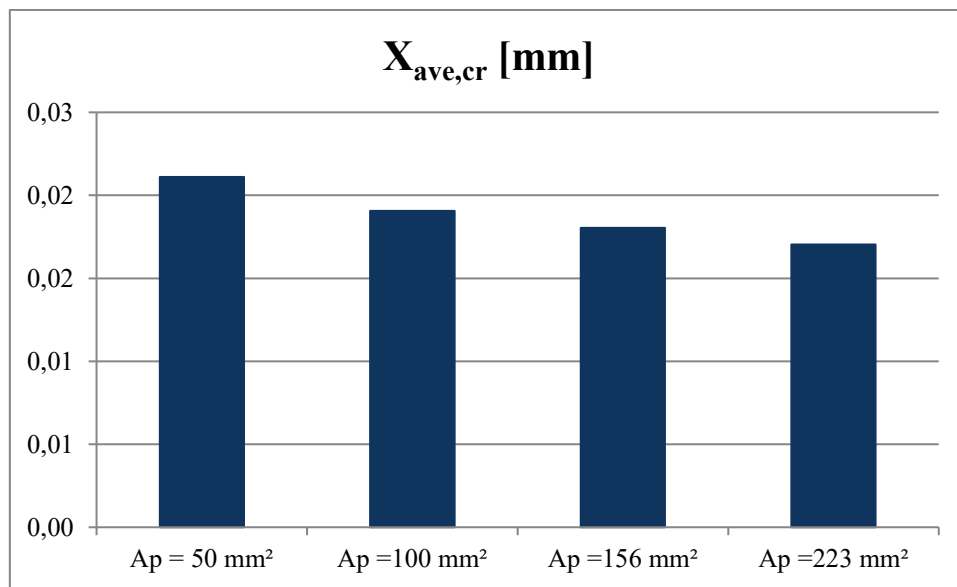


Figure 5.18 Critical corrosion penetration calculated for four strand areas

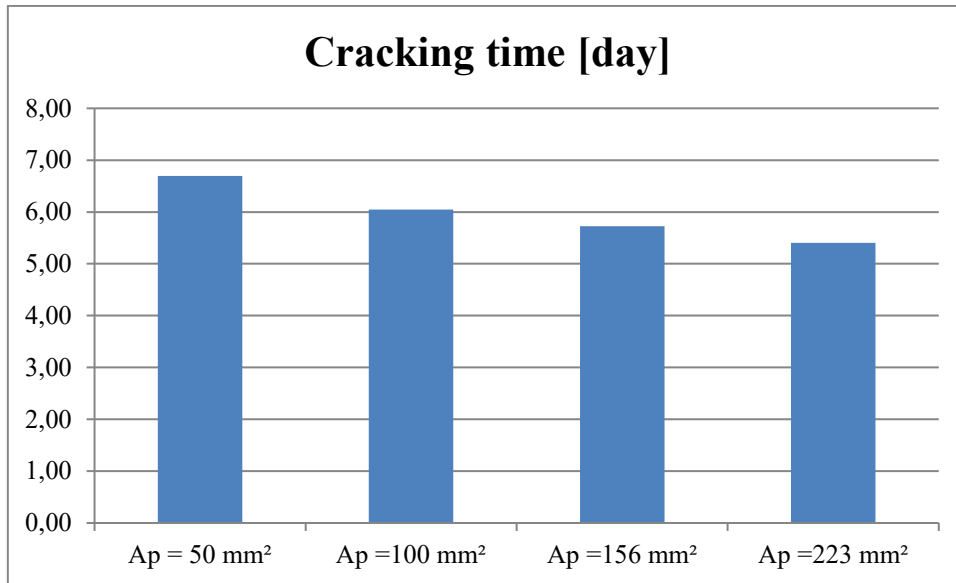


Figure 5.19 Time necessary to cracking calculated for four strand areas

It is clear that considering a larger strand area little corrosion is needed to get to the formation of the first crack, so a larger strand will crack in less time than a smaller strand.

5.7.2. Abacus to assess the level of corrosion in PC elements

An important tool that can be obtained using the analytical model studied is the abacus shown in the figure 5.20

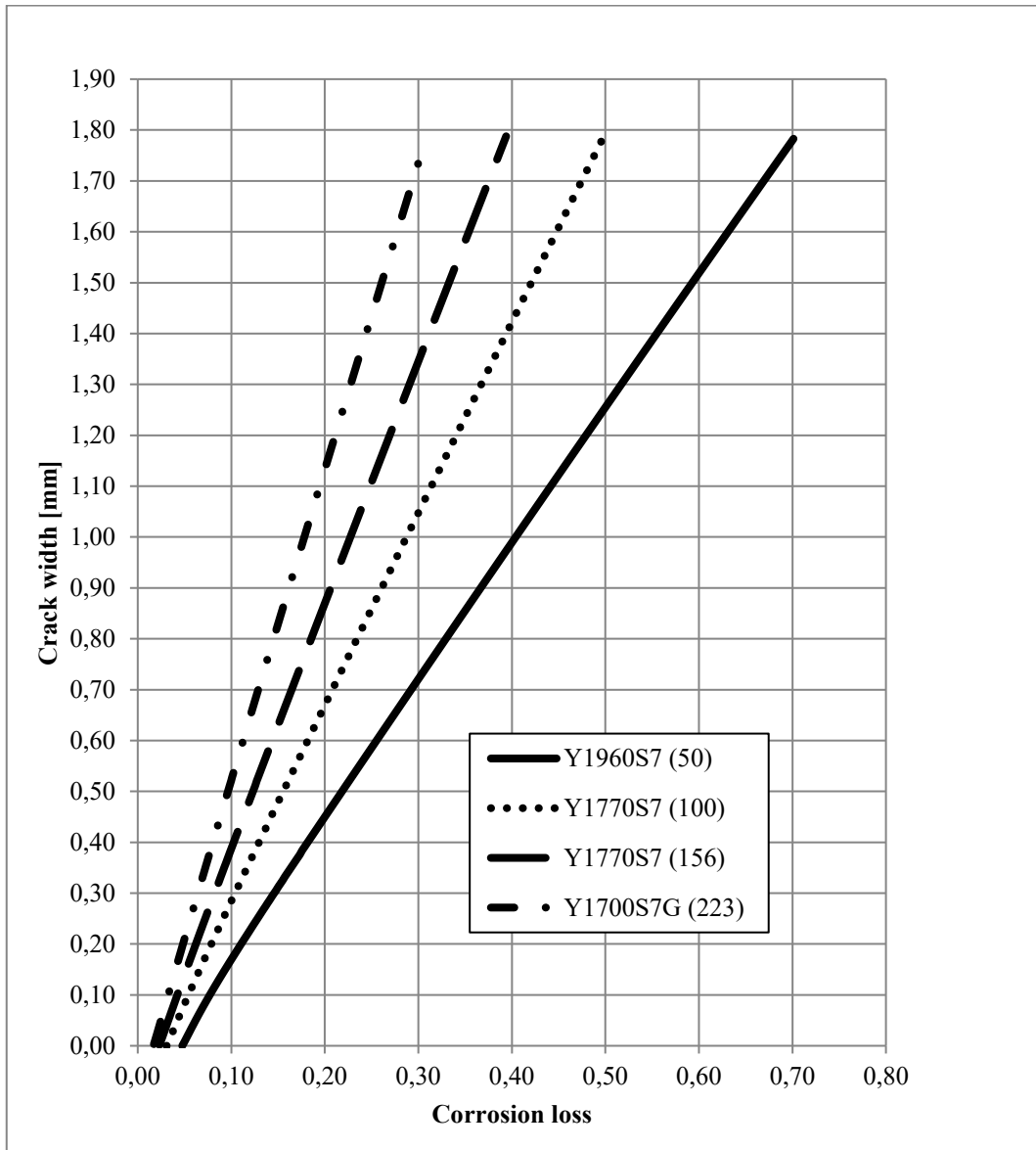


Figure 5.20 Abacus crack width-corrosion loss in PC elements

The abacus can be used in two ways:

- if the structure to be analysed is already deteriorated and cracks are visible, the corrosion loss relative to a specific strand area can be estimated from the crack width as shown in the Figure 5.21;
- A second use, as shown in the figure 5.22, is related to the optimization of the sections: according to the years it is possible to evaluate the cracks and see if they fall within the conditions of serviceability limit state.

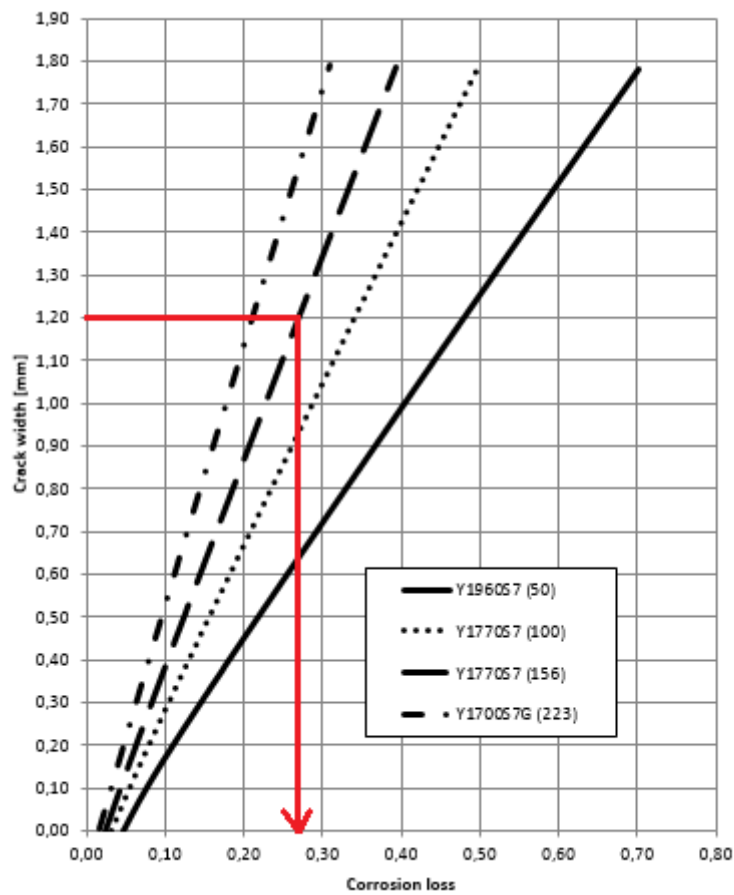


Figure 5.21 Evaluation of corrosion loss in relation to several A_p

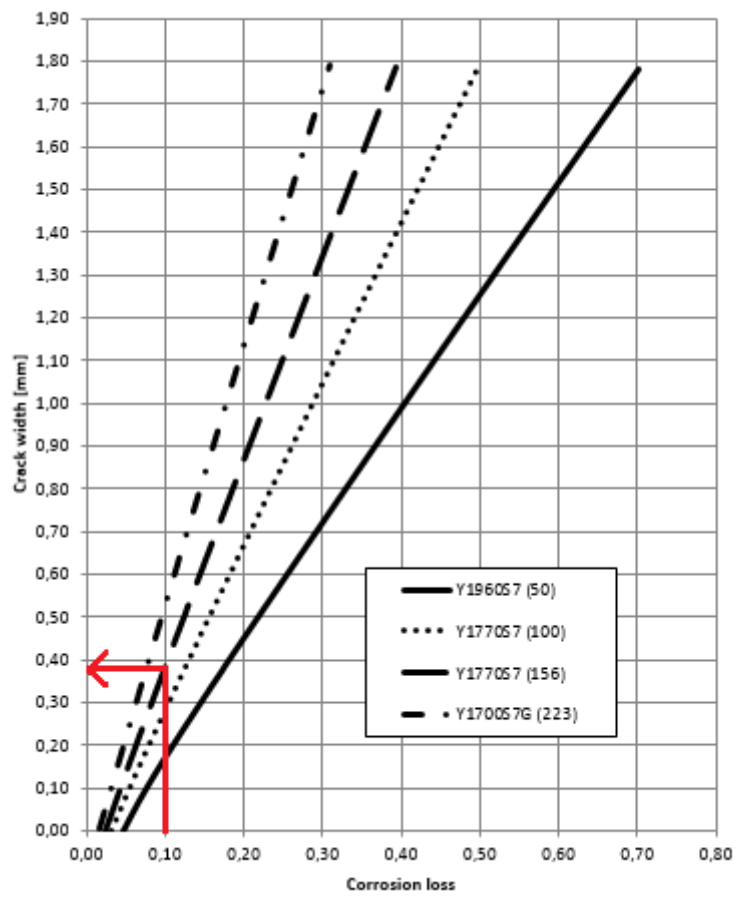


Figure 5.22 Evaluation of the crack width in relation to several Ap

CONCLUSIONS

The evaluation of the existing buildings' safety and therefore the analysis of the degradation of these structures is a fundamental aspect in the field of civil engineering.

Until the 1970s it was believed that concrete was not affected by durability problems, so reinforced concrete works were carried out with the conviction that they could last forever. In reality, concrete is not indestructible, but rather a material subjected to degradation, due to causes that can be mechanical, physical, structural, chemical and biological. Among these, one of the processes that has the greatest influence on the deterioration of concrete and on the degradation of reinforced concrete works is the corrosion of reinforcing bars.

A key concept is therefore the durability of reinforced concrete structures or the ability to guarantee the service for which the structure is designed and the relative safety for the expected life period.

From the early 1900s, in order to reduce the tensile stress present in the concrete, prestressing technique was introduced: stress induced in the structure to improve the structural behavior. Although the prestressed reinforcing bars are very sensitive to corrosion, studies concerning the cracking due to corrosion in prestressed reinforced concrete structures are lower if compared with those for ordinary reinforced concrete structures.

This thesis has had as main objective to analyse and test from the experimental point of view the various models present in the literature relating to RC and PC structures.

The first chapter is introductory and describes the importance of the conglomerate-steel bond and the effect of prestressing in the structures.

At the beginning of the second chapter the concept of structure durability is introduced and the main cause of deterioration of the structures is described: the

corrosion of the reinforcements. The main environmental factors that promote the corrosion process, such as carbonation and the presence of chlorides, are described.

There are several techniques for diagnosing degraded structures and the third chapter is dedicated to them where destructive methods are distinguished from non-destructive methods.

Among the various studies present in the literature, analysed in chapter 4, we focused in particular on the model introduced by Wang et al. (2019). The model analyses the global cracking process induced by corrosion, from the beginning up to the propagation. The relationship between corrosion loss and crack width was analyzed considering 4 levels of prestressing: 0, 0.25fp, 0.5fp and 0.75fp.

The model has been implemented in the MATLAB language and has been tested for both RC structures and PC structures.

The model applied to the RC structures was compared with the experimental results obtained by Andrade (1993) and Cesetti (2017): from the analyses carried out it was found that the analytical model strongly depends on the volumetric expansion coefficient n and therefore on the corrosion rate. Comparing the analytical model with the experimental results analysed in Cesetti (2017) it can be seen that the model is located inside the upper and lower curves, but for high values of corrosion there is an overestimation of the widths of the cracks.

The considerations related to the application of the analytical model in PC structures are the following: the implemented analytical model is more reliable close to the cracking condition, in fact the experimental data present in the literature show a plateau from a certain level of corrosion that the model cannot estimate.

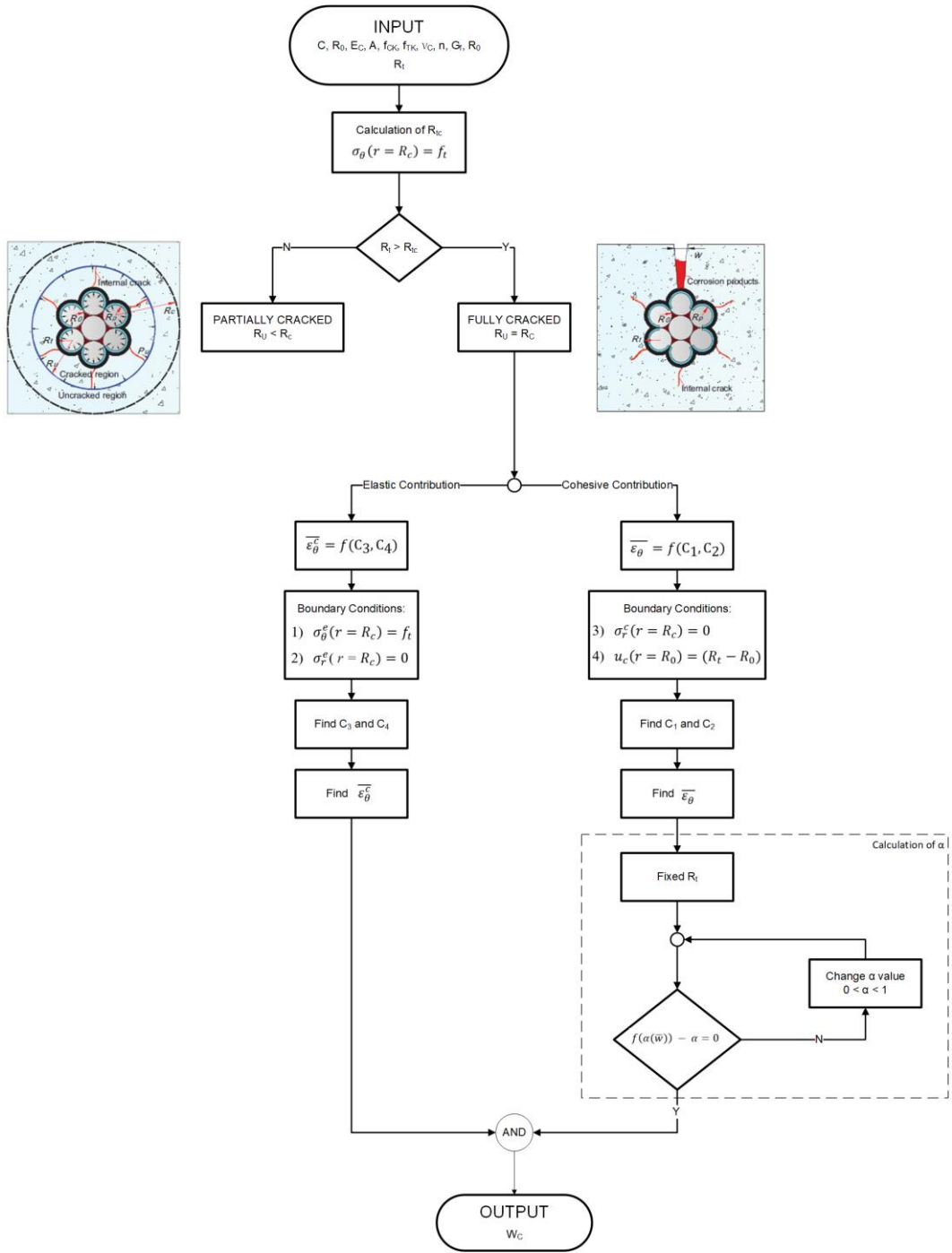
The prestressing accelerates the speed of propagation of the opening by about 9% so in the diagnostics it affects little the formation of the cracks. Two important applications of the model in the case of prestressed concrete structures are:

- to estimate the time required for the first visible crack to be formed according to the penetration depth;
- use the abacus to obtain the corrosion loss as a function of a certain crack width and vice versa to estimate the width of the cracks as a function of time.

The implemented analytical model can be a useful tool in monitoring operations and therefore in the evaluation of the crack widths within the service limits states.

A possible development of the aforementioned model could concern the study of the path taken by the oxides around the steel bar and therefore the evaluation of the threshold exceeded which the crack width no longer increase. In particular, greater importance should be given to the presence of a high concrete cover and to the possible dispersion of the oxide in the secondary cracks.

APPENDIX



ACKNOWLEDGMENTS

INDEX OF FIGURES

FIGURE 1.1 PRESTRESS EFFECT ON A SUPPORTED BEAM [9]	8
FIGURE 2.1 SIMPLIFIED MECHANISM OF STEEL CORROSION IN AQUEOUS MEDIUM: ANODIC E CATHODIC ZONE	12
FIGURE 2.2 EXAMPLE OF DEGRADATION DUE TO CORROSION [16].....	13
FIGURE 2.3 EVOLUTION OF THE CARBONATED FRONT AS A FUNCTION OF K AND T	14
FIGURE 2.4 DETERMINATION OF THE CARBONATED FRONT USING THE PHENOLPHTHALEIN TEST	15
FIGURE 2.5 DEPTH OF CORROSION PENETRATION.....	16
FIGURE 2.6 CARBONATION SPEED ACCORDING TO RELATIVE HUMIDITY.....	16
FIGURE 2.7 CORROSION INITIATION PROCESS [8]	19
FIGURE 2.8 PITTING CORROSION [8].....	19
FIGURE 3.1 EXAMPLE OF POTENTIAL MAPPING.....	26
FIGURE 3.2 SCHEMATIC ILLUSTRATION OF LINEAR POLARIZATION MEASUREMENTS.....	27
FIGURE 3.3 SCLEROMETRIC TESTS [15]	29
FIGURE 3.4 ULTRASONIC TESTS PERFORMED ON THE SPECIMENS [15]	31
FIGURE 3.5 PACOMETRIC TEST [15]	31
FIGURE 3.6 SONREB METHOD [15].....	32
FIGURE 3.7 PULL-OUT TEST [15]	33
FIGURE 3.8 CONCRETE SAMPLES TAKEN BY CORING	34
FIGURE 4.1 STRESS DISTRIBUTION AROUND THE STRAND-CONCRETE INTERFACE [4]	36
FIGURE 4.2 RADIAL DEFORMATION AT THE STRAND-CONCRETE INTERFACE [4].....	37
FIGURE 4.3 SCHEME OF COVER CRACKING [4]	38
FIGURE 4.4 SCHEMATIC OF CRACK WIDTH GROWTH [4].....	39
FIGURE 4.5 ACCELERATED CORROSION TEST OF BEAMS [4].....	40
FIGURE 4.6 FAILURE LOAD OF SPECIMENS [4]	41
FIGURE 4.7 THE EXPERIMENTAL AND PREDICTED CRACK WIDTHS [4]	41
FIGURE 4.8 DETAILS OF THE BEAM [MM] [5]	43
FIGURE 4.9 EXPANSIVE DEFORMATION AT THE STRAND-CONCRETE INTERFACE (MICRO CRACK FORMATION) [5].....	44
FIGURE 4.10 SIMPLIFIED CRACK MODEL [5].....	45
FIGURE 4.11 RUST FILLING RATIO AND CRACK WIDTH [5].....	47
FIGURE 5.1 DETAILS OF THE BEAMS [MM] [1].....	49
FIGURE 5.2 ACCELERATED CORROSION DEVICE [1].....	50

FIGURE 5.3 CRACK PROPAGATION OVER TIME FOR GROUPS A,B AND C [1]	52
FIGURE 5.4 CRACK WIDTHS AND CORROSION LOSSES UNDER VARIOUS PRESTRESS [1]	53
FIGURE 5.5 STRESS DISTRIBUTION AROUND THE STRAND-CONCRETE INTERFACE IN PC BEAMS [1]	54
FIGURE 5.6 CONCRETE CRACKING DUE TO STRAND CORROSION [1]	54
FIGURE 5.7 POSTCRACK STRESS AND CRACK WIDTH RELATIONSHIP (DATA FROM SHAH ET AL. 1995)	58
FIGURE 5.8 CRACK PROPAGATION TO THE CONCRETE SURFACE [1]	63
FIGURE 5.9 TYPE OF REINFORCED CONCRETE BEAM FABRICATED FOR THE EXPERIMENTATION [7]	66
FIGURE 5.10 LOSS IN BAR CROSS-SECTION VERSUS THE CRACK WIDTH MEASURED IN THE COVER. SPECIMENS WITH A CONCRETE COVER OF 20 MM.....	68
FIGURE 5.11 LOSS IN BAR CROSS-SECTION VERSUS THE CRACK WIDTH MEASURED IN THE COVER. SPECIMENS WITH A CONCRETE COVER OF 30 MM.....	68
FIGURE 5.12 EVALUATION OF THE ANALYTICAL MODEL BY VARYING THE VOLUMETRIC EXPANSION COEFFICIENT	69
FIGURE 5.13 CRACK WIDTHS AS A FUNCTION OF NORMALIZED CORROSION PENETRATION FOR THE MODIFIED COLLECTED DATA [6].....	74
FIGURE 5.14 VALIDITY OF THE ANALYTICAL MODEL STUDIED	75
FIGURE 5.15 EVALUATION OF THE ANALYTICAL MODEL WITH RESPECT TO CESETTI'S EXPERIMENTAL DATA.....	76
FIGURE 5.16 COMPARISON BETWEEN EXPERIMENTAL DATA AND ANALYTICAL MODEL: FIRST LEVEL OF PRESTRESSING.....	77
FIGURE 5.17 COMPARISON BETWEEN EXPERIMENTAL DATA AND ANALYTICAL MODEL: FOURTH LEVEL OF PRESTRESSING.....	78
FIGURE 5.18 CRITICAL CORROSION PENETRATION CALCULATED FOR FOUR STRAND AREAS	79
FIGURE 5.19 TIME NECESSARY TO CRACKING CALCULATED FOR FOUR STRAND AREAS	80
FIGURE 5.20 ABACUS CRACK WIDTH-CORROSION LOSS IN PC ELEMENTS.....	81
FIGURE 5.21 EVALUATION OF CORROSION LOSS IN RELATION TO SEVERAL A_p	82
FIGURE 5.22 EVALUATION OF THE CRACK WIDTH IN RELATION TO SEVERAL A_p	83

INDEX OF TABLES

TABLE 1 EXPECTED LIFE PERIOD [9].....	10
TABLE 2 CLASSIFICATION OF CORROSION LEVELS PROPOSED BY THE UNI EN 206 STANDARD	17
TABLE 3 ACCELERATED TIME OF SPECIMENS [5]	43
TABLE 4 CHEMICAL COMPOSITION OF STEEL [1]	48
TABLE 5 MECHANICAL CHARACTERISTIC OF STEEL [1].....	48
TABLE 6 TYPE OF BEAM [1]	49
TABLE 7 CRITICAL TIME OF COVER CRACKING [1]	52
TABLE 8 PARAMETERS OF CORROSION PRODUCTS [1]	55
TABLE 9 EMPIRICAL PARAMETERS FOR CORROSION DETERMINATION [6]	71
TABLE 10 EXPERIMENTAL TEST STATISTICALLY ANALYSED BY THE AUTHORS [14]	73

BIBLIOGRAPHY

- [1] Lei Wang, Lizhao Dai, Hanbing Bian, Yafei Ma & Jianren Zhang (2019). “Concrete cracking prediction under combined prestress and strand corrosion”.
- [2] Pantazopoulou and K.D. Papoulia, Members, ASCE (2001). “Modeling cover cracking due to reinforcement corrosion in RC structures”.
- [3] C.Q. Li and S.T. Yang (2011). “Prediction of concrete crack width under combined reinforcement corrosion and applied load”.
- [4] Lizhao Dai, Lei Wang, Jianren Zhang, Xuhui Zhang (2016). “A global model for corrosion-induced cracking in prestressed concrete structures”.
- [5] Lei Wang, Lizhao Dai, Xuhui Zhang and Jianren Zhang (2016). “Concrete cracking prediction including the filling proportion of strand corrosion products”.
- [6] A. Cesetti (2017). “Effect of corroded reinforcement in RC structures: From cracking to bond performance”.
- [7] C. Andrade, C. Alonso, F.J. Molina (1993). “Cover cracking as a function of rebar corrosion: Part 1-Experimental test, Part 2-Numerical model”.
- [8] AICAP e Pietro Pedferri (2015). “La corrosione nel calcestruzzo-Fenomenologia, prevenzione, diagnosi e rimedi”.
- [9] L. Giordano, lezioni del corso di Teoria e progetto delle costruzioni in c.a. e c.a. precompresso, Politecnico di Torino (2018).
- [10] Alonso, C., Andrade, C., Rodriguez, J., and Diez, J., “Factors controlling cracking of concrete affected by reinforcement corrosion”, *Materials and Structures/Materiaux et Constructions*, vol. 31, no. 211, pp. 435–441, (1996).
- [11] Rodriguez, J., Ortega, L., Casal, J., and Diez, J., “Corrosion of reinforcement and service life of concrete structures”, in: *Proceedings of the Seventh*

International Conference on Durability of Building Materials and Components, London, UK, (1996), pp. 117–126.

[12] Alonso, C., Andrade, C., Rodriguez, J., and Diez, J., “Factors controlling cracking of concrete affected by reinforcement corrosion”, *Materials and Structures/Materiaux et Constructions*, vol. 31, no. 211, pp. 435–441, (1996).

[13] Vidal, T., Castel, A., and François, R., “Analysing crack width to predict corrosion in reinforced concrete”, *Cement and Concrete Research*, vol. 34, no. 1, pp. 165–174, (2004).

[14] Andrade, C., Cesetti, A., Mancini, G., and Tondolo, F., “Estimation of corrosion attack in reinforced concrete by means of crack opening”, *Structural Concrete*, vol. 17, no. 4, pp. 533–540, (2016).

[15] Sito Web: <https://diagnosticastrutturale.it/>.

[16] Sito Web: <http://rivista.inarcassa.it/1-2019/professione/dopo-il-crollo-del-ponte-di-genova-nasce-il-siscon.>